iScience

CellPress
OPEN ACCESS

Article

Regenerative potential of mouse neonatal intervertebral disc depends on collagen crosslink density

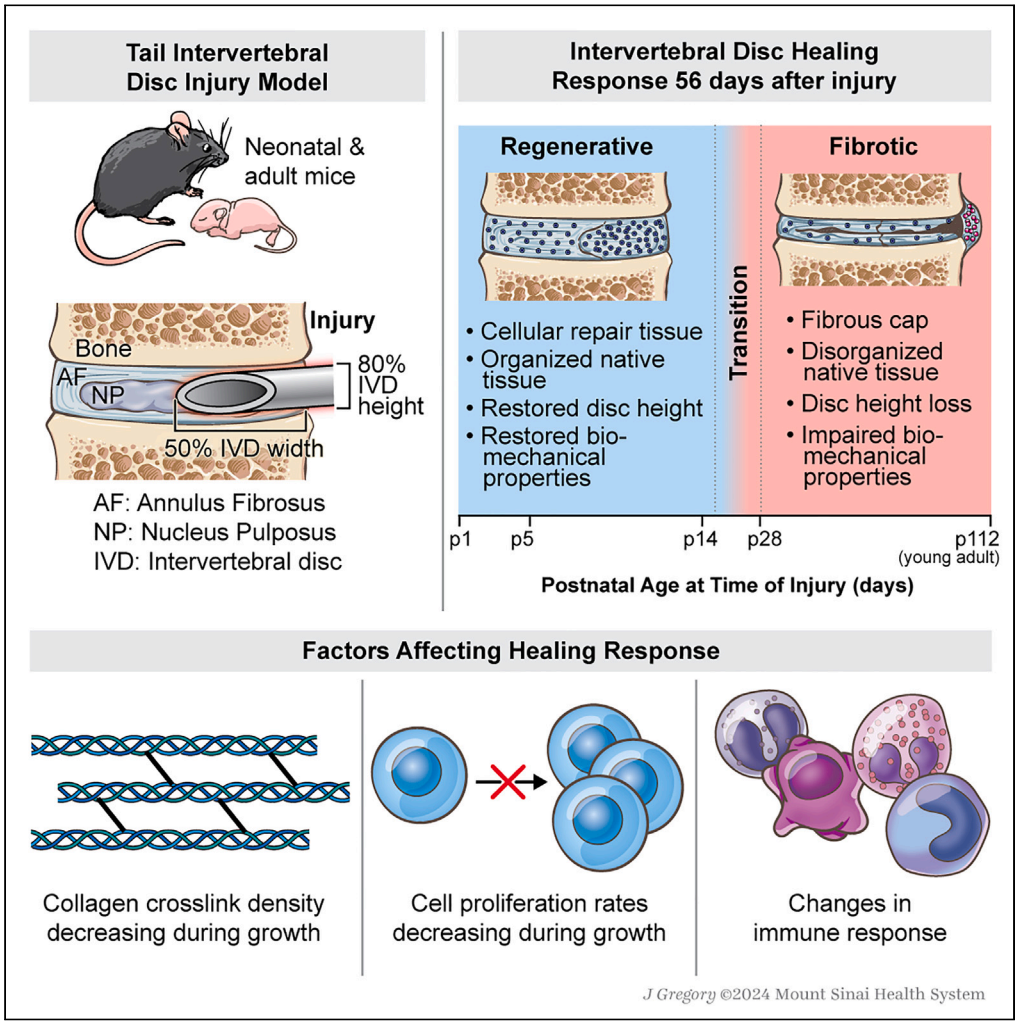

Danielle N. D'Erminio, Kaya A. Adelzadeh, Ashley M. Rosenberg, ..., Woojin M. Han, Alice H. Huang, James C. Iatridis

james.iatridis@mssm.edu

Highlights

Mouse disc regenerative healing window closes between postnatal days 14 & 28

Disc growth shifts from cell proliferation to matrix elaboration at postnatal day 14

Full structural regeneration after herniation is not possible in discs of any age

Reduced collagen crosslinking during growth shifted disc regeneration to fibrosis

D'Erminio et al., iScience 27, 110883
October 18, 2024
https://doi.org/10.1016/j.isci.2024.110883

iScience

CellPress
OPEN ACCESS

Article

Regenerative potential of mouse neonatal intervertebral disc depends on collagen crosslink density

Danielle N. D'Erminio,[1,2] Kaya A. Adelzadeh,[1] Ashley M. Rosenberg,[1] Robert J. Wiener,[3] Olivia M. Torre,[1] Emily D. Ferreri,[1] Philip Nasser,[1] Kevin D. Costa,[3] Woojin M. Han,[1] Alice H. Huang,[4] and James C. Iatridis[1,5,*]

SUMMARY

Intervertebral disc (IVD) defects heal poorly and can cause back pain and disability. We identified that IVD herniation injury heals regeneratively in neonatal mice until postnatal day 14 (p14) and shifts to fibrotic healing by p28. This age coincides with the shift in expansive IVD growth from cell proliferation to matrix elaboration, implicating collagen crosslinking. β-aminopropionitrile treatment reduced IVD crosslinking and caused fibrotic healing without affecting cell proliferation. Bulk sequencing on naive IVDs was depleted for matrix structural organization from p14 to p28 to validate the importance of crosslinking in regenerative healing. We conclude that matrix changes are key drivers in the shift to fibrotic healing, and a stably crosslinked matrix is needed for IVD regeneration.

INTRODUCTION

Intervertebral discs (IVDs) are fibrocartilaginous tissues located between each vertebrae providing flexibility and stability to the spinal column. Large spinal loads are supported by the complex IVD structure consisting of the pressurized nucleus pulposus (NP) that is constrained peripherally by the lamellar collagen of the annulus fibrosus (AF), and confined on top and bottom surfaces by cartilaginous endplates.[1,2] IVDs heal poorly in humans causing IVD degeneration and back pain, a leading cause of disability costing > $130 billion in the U.S..[3,4] AF defects can cause disability from biomechanical instability and herniation, where the NP tissue extrudes out of AF defects to cause neuropathy.[5,6] Discectomy surgery removes herniated NP tissue compressing surrounding nerves but leaves AF defects unrepaired and susceptible to reherniation, progressive IVD degeneration, and recurrent pain.[5] AF closure devices limit reherniation, but do not promote AF repair, risk subsidence with adjacent tissue damage, and are in limited clinical use.[7,8] We believe *in vivo* models of IVD regeneration are needed to provide a roadmap of natural IVD healing to inform improved repair methods.

Surprisingly few IVD regeneration studies exist considering the enormous socioeconomic impact of disabling IVD degeneration and back pain. Neonatal mice are an attractive mammalian model used to show cardiac regeneration occurs by expansion of resident cardiomyocytes and tendon regeneration occurs by the recruitment and proliferation of tenocytes.[9,10] In the IVD, severe herniation injuries in postnatal day 5 (p5) mice functionally regenerate with extensive matrix deposition, and with restored IVD height and biomechanical function, but without the recapitulation of the AF structure.[11] Meanwhile, herniation injuries in skeletally adult mice (4–6 months) heal with fibrotic scarring, loss of IVD height, inferior biomechanical properties, and little matrix deposited within injury sites.[11] With so few studies on IVD regeneration, there remain an abundance of open questions.

As neonatal murine IVDs mature skeletally, the AF undergoes changes in composition, structure, and cellularity,[12,13] and some of these factors could be important in IVD regenerative healing. Postnatal murine IVD growth is driven by cell proliferation at early postnatal periods followed by the deposition and accumulation of collagens and proteoglycans at later times.[12,13] Therefore, changes in IVD cell proliferation and matrix deposition may limit IVD regenerative potential. Large alterations in collagen content and organization during growth[14] are also likely to influence IVD regenerative potential,[15] yet changes in AF collagen deposition, crosslinking density, and matrix elastic modulus in early growth are largely underexplored. In tendons, collagen crosslinking density is a measure of tendon mechanical function during development,[16,17] suggesting its importance for tissue formation. Interestingly, collagen crosslinking density is also implicated in regenerative healing since cardiac regeneration was restored in neonatal mice by pharmacologically inhibiting collagen crosslinking with β-aminopropionitrile (BAPN).[15] Reduced crosslinking provides a softer extracellular matrix that could alter cell differentiation or transport patterns, enabling matrix

[1]Department of Orthopedics, Icahn School of Medicine at Mount Sinai, New York, NY, USA
[2]Department of Biomedical Engineering, The City College of New York at CUNY, New York, NY, USA
[3]Cardiovascular Research Institute, Icahn School of Medicine at Mount Sinai, New York, NY, USA
[4]Department of Orthopedic Surgery, Columbia University, New York, NY, USA
[5]Lead contact
*Correspondence: james.iatridis@mssm.edu
https://doi.org/10.1016/j.isci.2024.110883

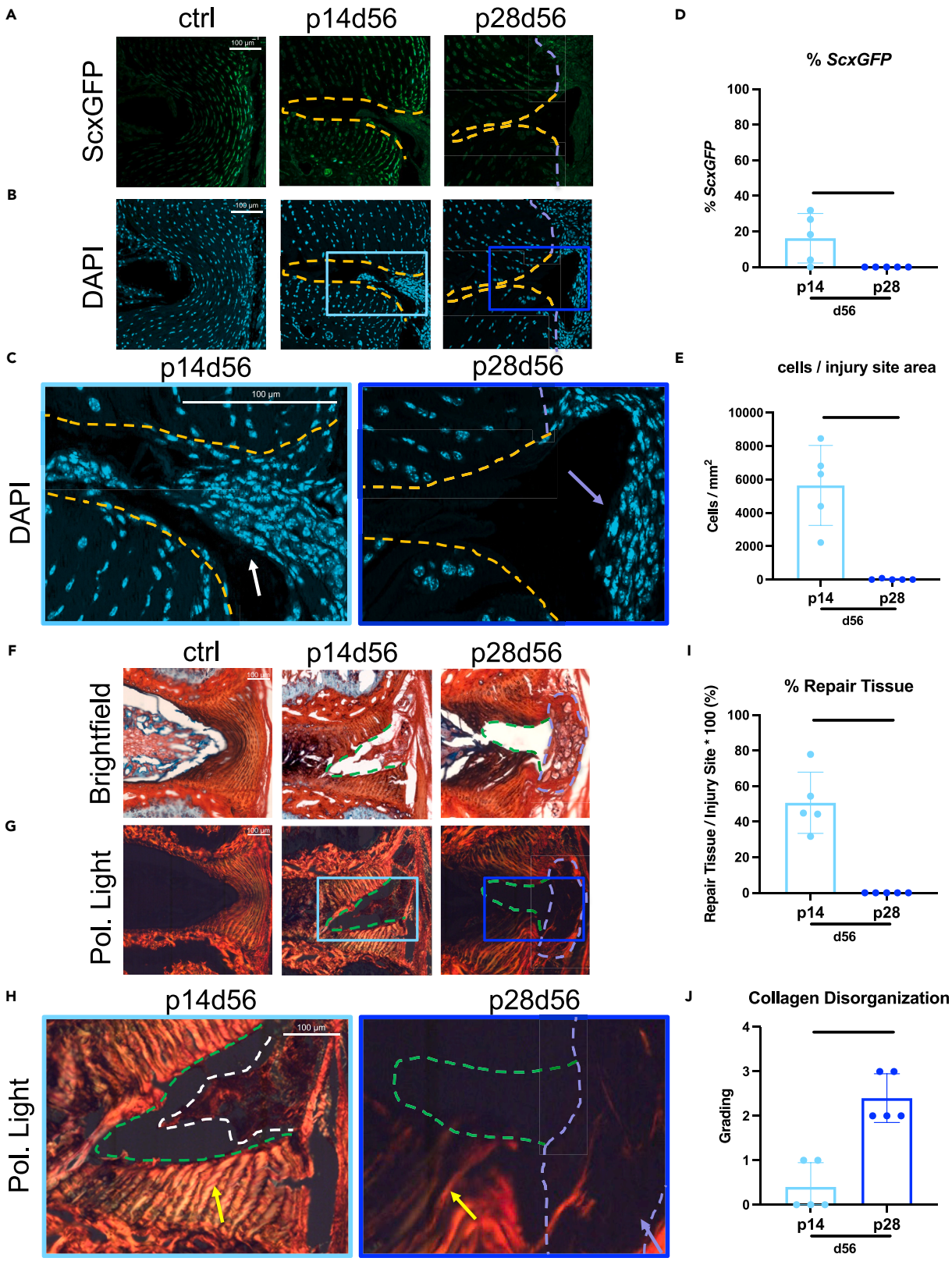
A
ctrl
p14d56
p28d56
ScxGFP
B
DAPI
C
p14d56
p28d56
DAPI
100 µm
D
% ScxGFP
% ScxGFP
100
80
60
40
20
0
p14
p28
d56
E
cells / injury site area
Cells / mm²
10000
8000
6000
4000
2000
0
p14
p28
d56
F
ctrl
p14d56
p28d56
Brightfield
G
Pol. Light
I
% Repair Tissue
Repair Tissue / Injury Site * 100 (%)
100
80
60
40
20
0
p14
p28
d56
H
p14d56
p28d56
Pol. Light
J
Collagen Disorganization
Grading
4
3
2
1
0
p14
p28
d56

Figure 1. Injured p14 IVDs heal regeneratively with highly cellular matrix deposition throughout the injury site and organized AF layers adjacent to the injury while injured p28 IVDs heal with fibrosis

(A–J) Representative (A) *ScxGFP* and (B) DAPI images of AF controls and injury sites of p14 and p28 mice 56 days after injury with (C) magnified images of injury sites with DAPI. Quantification of (D) % cells expressing *ScxGFP* and (E) total number of cells within injury sites. Picrosirius Red Alcian blue images of AF controls and injury sites of p14d56 and p28d56 mice under (F) brightfield and (G) polarized light with (H) magnified images of injury sites of p14d56 and p28d56. Quantification of (I) % repair tissue within the injury site and (J) collagen disorganization score. Scale bars = 100 μm. Dashed lines outline injury sites (yellow or green), fibrous caps (purple), and repair tissue (white). Arrows point toward cellular repair tissue (white), fibrous caps (purple), and adjacent AF structures near injury sites (yellow). Biological n = 5/age, error bars = SD. Student's t test with $p < 0.05$ determined significance, depicted in graphs as a horizontal black line.

repair processes to occur more effectively.[18,19] IVD matrix changes during early growth are also likely to influence regenerative healing potential, yet there are no studies evaluating this relationship.

Very few studies on IVD regenerative healing exist motivating this multi-part study to answer several key open questions in IVD regeneration. We first applied herniation-type injuries to mouse coccygeal IVDs of varying ages from p1 to p28 and skeletally mature adults to determine when the IVD regenerative window closes in neonatal mice and whether full AF structural regeneration occurs in IVD-herniation injury at the earliest postnatal ages. We also performed a neonatal IVD growth study to characterize cell proliferation and extracellular matrix changes during the period when the IVD regenerative window closes. Having identified the shift from regenerative to fibrotic IVD healing coincides with the neonatal age when expansive growth shifts from cell proliferation to matrix elaboration, we determined what matrix factors are important for IVD regeneration by pharmacologically inhibiting collagen crosslinking and evaluating changes in IVD healing. All studies applied a neonatal mouse model with relevant measurements of IVD structure, cells, composition, and macro- and micro-mechanical properties. We also validated our findings with bulk RNA sequencing for an unbiased evaluation of the most important changes occurring when IVD healing shifts from regenerative to fibrotic healing.

RESULTS

Intervertebral discs with annulus fibrosus herniation injuries healed with improved structure at postnatal day 14but with fibrosis at p28

At day 3 post-injury (d3) and with Picrosirius red Alcian blue (PRAB) staining, injured IVDs had comparable severities when induced in p5, p14, and p28 mice (Figure S1C, Top). Specifically, large-sized AF herniation injuries resulted in herniated NP tissue, collapsed disc height, and disrupted AF structure but had some remaining native AF tissue adjacent to the injury sites. There was greater severity when induced in p1 mice with very little AF tissue remaining around injury sites in p1d3 IVDs (Figure S1C, Top). Uninjured control IVDs at d3 had healthy hydrated NP tissue, distinct boundaries between AF and NP, and concentrically organized AF lamellae (Figure S1C, Bottom).

IVD healing of p14 and p28 mice characterized 56 days post-injury (d56) (Figure 1) were analyzed for DAPI, *ScxGFP, and* for Scx, a transcription factor expressed in tendons, ligaments, and the AF allowing *ScxGFP* to be used as an AF phenotypic marker and to help visualize the AF for injury creation.[11,20] Uninjured control IVDs at d56 showed organized concentric layers of cells of the AF with *ScxGFP* expression brightest at the outer layers. The p14d56 IVDs revealed high cellular repair tissue ingrowth within injury sites (Figures 1B–1E) with some cells exhibiting *ScxGFP* positivity (Figures 1A and 1D). In contrast, p28d56 IVDs had significantly less cellularity with almost no cells within injury sites inside the boundary of native AF tissue and no cells exhibiting *ScxGFP* positivity (Figures 1D and 1E). The p28d56 mice healed with highly cellular fibrotic tissue outside of the periphery of the IVD space (Figures 1B and 1C).

Uninjured control discs displayed healthy IVD characteristics with hydrated NP tissue, clear NP/AF boundaries, and organized AF structure with PRAB stained slides with brightfield and polarized light imaging (Figure 1F). The p14d56 IVDs had extensive red-stained repair tissue within the injury sites indicating collagen deposition (Figure 1F). In contrast, the p28d56 IVDs healed with a red-stained matrix deposited on the outer edge of the IVD, indicating a fibrotic cap, but no repair tissue in the injury site (Figure 1F). The p28d56 injury IVDs had significantly less % Repair Tissue than the p14d56 injury IVDs (Figure 1I). The collagen organization of repair tissue and integrity of AF lamellar fibers immediately adjacent to the injury sites were evaluated and quantified (Figures 1G–1J and S2). In p14d56 IVDs had AF repair tissue with birefringence indicating some organization of the newly deposited collagen (Figure 1H), and AF layers immediately adjacent to the injury sites were bright red/orange indicating retained and highly organized collagen with low collagen disorganization scores (Figures 1J and S2). In contrast, AF fibers in p28d56 injured discs exhibited a gradient from bright to darker and greener in color closer to the injury sites indicating matrix degradation, and significantly higher collagen disorganization score (Figures 1H and 1J). The fibrotic cap at the outer edge of p28d56 IVDs was dark under polarized light indicating little structural organization (Figure 1H). Histological assessments therefore identified that p14d56 healing was near-regenerative with highly cellular and organized AF repair tissue within the injury site, and retained adjacent AF layers while p28d56 healing involved a fibrotic cap, little AF repair tissue, and disrupted adjacent AF layers.

Disc height and biomechanical function were restored in p14d56 mice but not in p28d56

Histological results prompted functional evaluations of IVD healing with disc height measurements and motion segment biomechanical testing (Figure 2). Because the fibrotic healing response in p28d56 was robust, we also investigated skeletally mature adult (p112-p168) IVDs with injury (i.e., adultd56) as a known non-regenerative age for comparison.[11] Disc height loss as measured on Faxitron X-rays is a sensitive marker for IVD disruption,[21,22] and disc height index (DHI) was calculated to control for differences in animal size (Figure 2A). DHI for

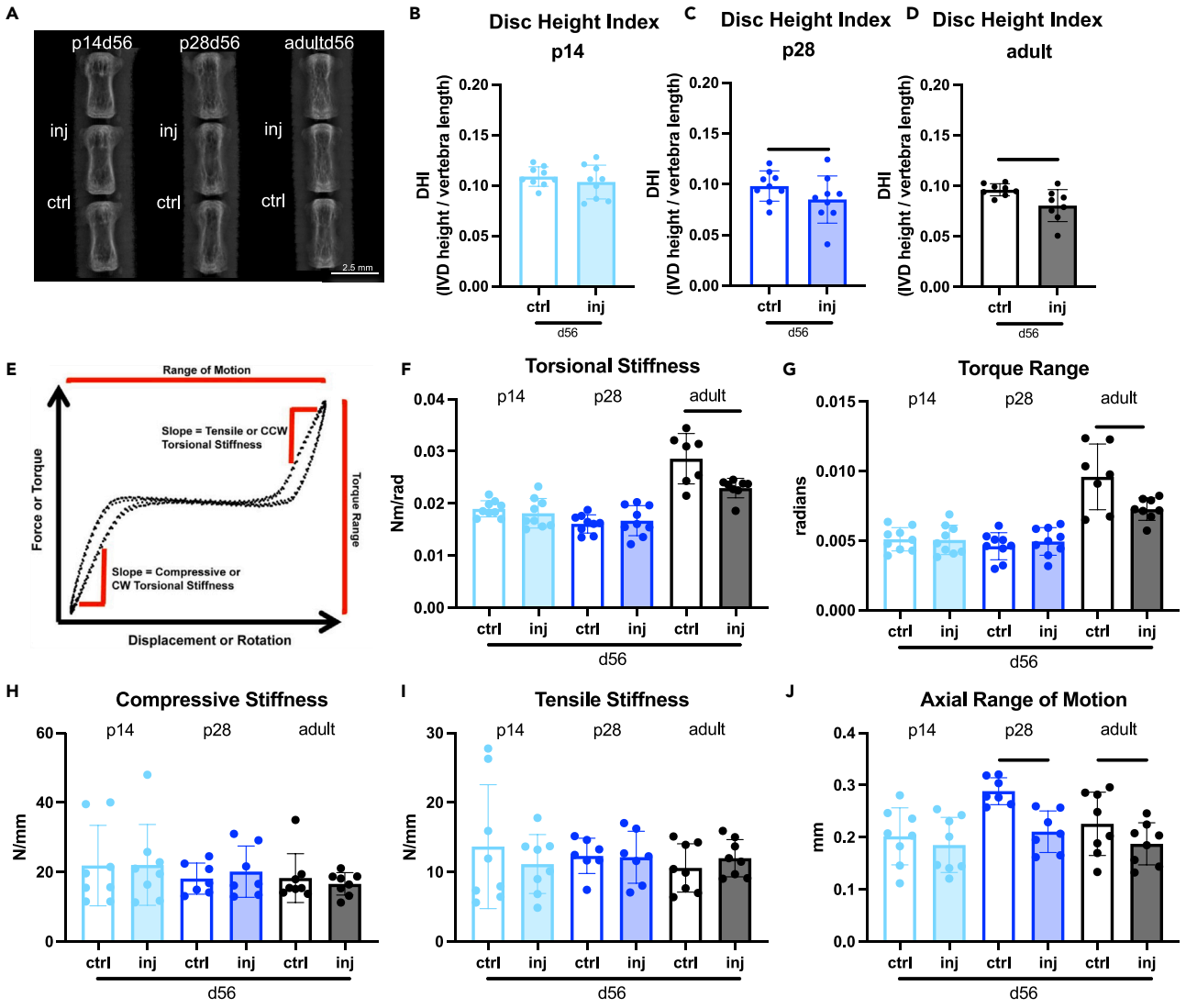

Figure 2. Injured p14 IVDs heal with restored disc height index (DHI) and biomechanical properties by d56 while injured p28 IVDs and adult IVDs do not

(A) digital X-rays used to calculate DHI in (B) p14, (C) p28, and (D) adult mice (biological n = 8–9/age) 56 days after injury. Scale bars represent 2.5 mm. (E) Representative loading curve for samples used to determine torsional (F and G) and (H–J) axial biomechanical parameters. Error bars = SD. Student's t test with $p < 0.05$ determined significant differences between ctrl and inj for each age, depicted in graphs as a horizontal black line.

injured p14d56 IVDs was comparable to the uninjured adjacent controls (Figure 2B), similar to p5d56 mice previously reported.[11] In contrast, the p28d56 and adultd56 IVDs had significantly decreased DHI (Figures 2C and 2D), supporting histological findings that p28 and older IVDs had inferior healing.

Control and injured motion segments at d56 post-injury were evaluated functionally with biomechanical testing. Parameters derived from loading curves from cyclic torsional testing are most sensitive to AF integrity while parameters from cyclic axial compression/tension testing are sensitive to both NP pressurization and AF integrity,[5] with parameter definitions and representative loading curves provided (Figures 2E and S3). Adultd56 injured IVDs had functionally inferior biomechanical behaviors with significantly reduced torsional stiffness, torque range, and axial range of motion, consistent with previous histology and biomechanical results.[11] There were no changes in torsional or axial biomechanical properties in p14d56 injured IVDs indicating robust functional healing with restored biomechanical function (Figures 2F–2J). Injured p28d56 IVDs had no changes in torsional properties which contrasted with adult healing, suggesting a more robust healing response (Figures 2F–2J). However, p28d56 had a significantly decreased axial range of motion, similar to adult healing, suggesting fibrotic healing may limit axial motion at this age (Figure 2J). Overall, p14d56 was functionally regenerative with restored DHI and biomechanical properties; p28d56 exhibited robust fibrotic healing with restored torsional properties but altered DHI and loss of axial motion; and adultd56 exhibited inferior healing with altered DHI, torsional, and axial biomechanical properties.

Structural regeneration did not occur with herniation injury at any postnatal ages

The p14d56 mice were near-regenerative and functionally restored yet did not fully recapitulate the herniated NP or AF lamellar structure. To determine if structural regeneration was possible in neonatal mice at earlier ages, p1 and p5 healing were evaluated. Similar to the p14d56 mice, fluorescent imaging of p1d56 and p5d56 injured IVDs revealed highly cellular tissue deposited within the AF boundary which contained some *ScxGFP* cells (Figures 3A and 3B). Both p1 and p5 had comparable % of cells exhibiting *ScxGFP* positivity and total cells within injury sites (Figures 3A–3D). Values were similar to p14d56 indicating highly cellular AF repair tissue, compared to no cells seen within injury sites in p28d56 mice. Healing of p1d56 and p5d56 also involved matrix deposition within injury sites with % Repair Tissue more similar to p14d56 than to p28d56 (which contained almost no repair tissue), yet p1d56 had significantly less % Repair Tissue than p5d56 animals (Figures 3E and 3F). However, the AF layers adjacent to the injury site were intact with bright birefringence under polarized light for p5d56 and p1d56 animals (Figure 3G), leading to low collagen disorganization scores similar to p14d56 (Figure 3H). The p1d56 and p5d56 demonstrated near regenerative healing histologically with highly cellular AF repair tissue, with neither fully recapitulating the NP or AF lamellar structure. We note, however, that injured p1d56 IVDs had significantly reduced DHI compared to controls (Figure 3I) unlike the p5d56 IVDs reported previously which did not lose DHI,[11] which we attribute to a greater injury severity in the p1 mice (Figure S1C). The small size of the p1 mice led to difficulty in controlling the injuries compared to the other older (and larger) neonatal mice. Specifically, PRAB of p1d3 revealed very little intact AF tissue remaining compared to p5 and older injuries (Figure S1C). We conclude that p1d56 and p5d56 healed near-regeneratively from large-sized AF herniation injury, yet no neonatal mice of any age were able to recapitulate the native NP or AF lamellar structure following this severe injury with NP herniation.

IVDs from injured p5 mice aged out to day 84 (p5d84) had tissue ingrowth similar to what was seen in p5d56. This indicates that d56 post-injury is a stable healing condition in this model system and that the AF injury site does not continue to remodel or restore its AF lamellar structure (Figure S4).

Expansive neonatal intervertebral disc growth involves a shift from cell proliferation to matrix deposition with significantly decreased crosslinking density as the regenerative window closes

Having identified that the IVD regenerative healing window closes from p14 to p28, we characterized major changes in cell proliferation and matrix elaboration during these ages to identify factors involved in the loss of IVD regenerative potential. Multiphoton imaging was used to measure collagen content (second harmonic generation (SHG), excitation 910 nm) and crosslinking (two photon excitation fluorescence (TPEF), excitation 720nm) in the AF as previously reported in embryonic chick tendon,[17] which is a similar fibrous connective tissue as the AF. During growth, the AF was increasingly dominated by organized and mature collagen that was particularly notable at p14 and continued to increase until skeletal maturity, as indicated by the increase in SHG signal and TPEF signal over time (Figures 4A–4C). When normalizing the crosslinking by the amount of collagen present (TPEF/SHG) there were high crosslinking density levels shortly after birth before significantly decreasing during early growth (Figure 4D). Atomic force microscope (AFM) nano-indentation measured the stiffness of outer AF tissue on intact IVDs from p1 to adult mice (Figure S5). AF elastic modulus (E) was lowest shortly after birth at p1 (~35 kPa), significantly increased at p5 (~50 kPa), and reached a steady state at p56 (~75 kPa) which was not significantly different than skeletally mature adult AF tissue (~75 kPa) (Figure 4E). Results therefore indicated the AF elastic modulus increased with neonatal growth; this corresponded with the increase in collagen content and crosslinking but contrasted with the decrease in crosslinking density.

Cell mitotic potential is reduced during growth and could be implicated in the loss of AF regenerative potential, so we assessed % proliferating AF cells at varying ages using immunohistochemistry for Ki67 as well as Edu (Figure 4F; Figures S6 and S7). The AF % cell proliferation was highest at p1 (~35%), remained high at p5 (30%), was significantly reduced by p14 (10%), and exhibited very little % cell proliferation by p28 and older (Figure 4F). The % proliferating NP and cartilage endplate cells had similar patterns as AF cells. The significant and substantial drop in % AF cell proliferation at p14 and again at p28 suggests it could be implicated in the loss of AF regenerative healing potential.

Overall, at p14 we observed a major shift in growth mechanisms from AF cell proliferation to collagen deposition, as measured by SHG intensity (Figure 4J). Furthermore, % cell proliferation and crosslinking density followed similar patterns substantially decreasing from birth to p14 and p28 (Figure 4K) prompting further investigation.

β-aminopropionitrile decreased collagen crosslinking density and impaired annulus fibrosus regeneration without altering cell proliferation

BAPN, a lysyl-oxidase inhibitor, was used to inhibit collagen crosslinking and was given to neonatal mice from embryonic day 5.5 until either p5 or p14 (Figure S1D). BAPN treated mice were compared to untreated age-matched control mice. Note untreated mice were the same as those used in the growth studies in the previous section since all mice were analyzed together, (Figure S1D). BAPN treatment significantly reduced the AF crosslinking density of p14 mice but not p5 mice (Figures 5A and 5C), with no other obvious changes in collagen SHG signal detected (Figure 5A). AFM nano-indentation was performed on p14 mice only since p5 mice did not exhibit any significant changes in crosslinking density due to BAPN treatment. AFM showed BAPN significantly reduced AF tissue modulus in p14 mice when compared to untreated age-matched controls (Figure 5D). BAPN treatment did not affect % cell proliferation as measured with DAPI and Ki67 (Figures 5B and 5E) and had no effect on vertebral length, IVD diameter, or number of lamellar AF layers on p14 mice (Figure S8A).

The p14BAPN treated mice received AF puncture at p14 and were evaluated at d56 (p14BAPNd56) to investigate whether decreased collagen crosslinking density and tissue modulus affected AF regenerative healing (Figure 6). Injured p14BAPNd56 IVDs exhibited a shift toward fibrotic healing with a significantly decreased number of cells in the injury site, % *ScxGFP*, and % repair tissue compared to the p14d56

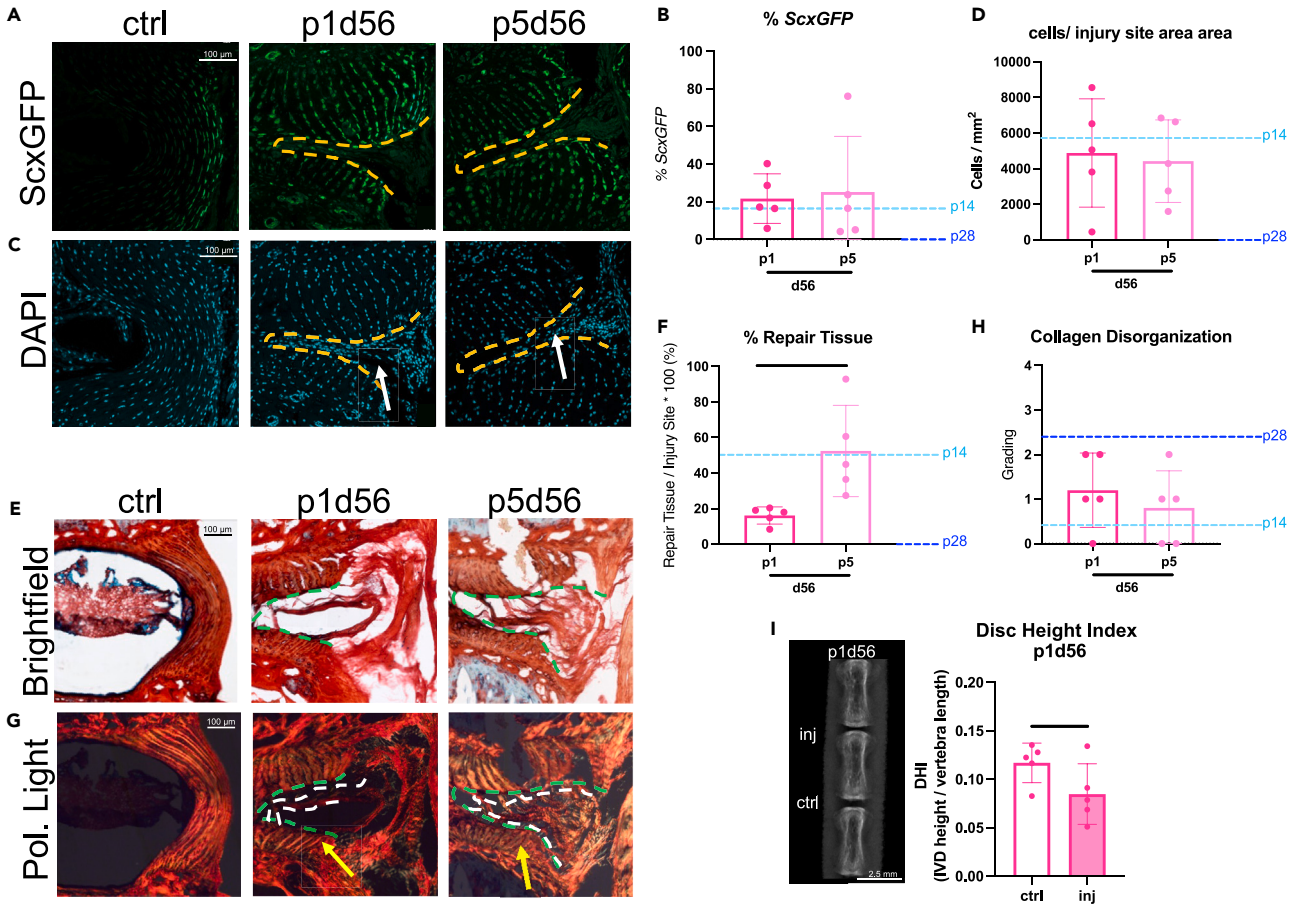

Figure 3. Injured p1 and p5 IVDs heal near-regeneratively suggesting neonatal IVD regeneration does not recapitulate the AF lamellar structure after a severe herniation-type injury at any post-natal age

(A and B) Representative (A) *ScxGFP* and (B) DAPI images of AF controls and injury sites of p1 and p5 mice (biological n = 5/age) 56 days after injury.

(C and D) Quantification of (C) % cells expressing *ScxGFP* and (D) total number of cells within injury sites.

(E and F) Representative Picrosirius Red Alcian blue images of AF controls and injury sites of p1d56 and p5d56 mice under (E) brightfield and (F) polarized light.

(G and H) Quantification of (G) % repair tissue within the injury site and (H) collagen disorganization score. Scale bars = 100 µm. Quantifications are compared to p14 and p28 levels marked by light and dark blue dotted lines respectively. Outlines indicate injury sites (yellow/green) and repair tissue (white).

(I) Arrows point toward cellular repair tissue (white) and adjacent AF structure near injury sites (yellow) (I) Digital X-rays are used to calculate DHI in p1 injured and control IVDs. Scale bars represent 2.5 mm. Error bars = SD. Student's t test with $p < 0.05$ determined significance, depicted in graphs as a horizontal black line.

functionally regenerative IVDs (Figures 6A–6F). Note the p14BAPNd56 mice were compared to the p14d56 mice used in the regenerative window study since all assessments were simultaneously performed (Figure S1D). The p14BAPNd56 IVDs had increased collagen disorganization score and fibrotic scarring at the periphery of the IVD with AF layers adjacent to the injury sites darker with less birefringence (Figures 6G and 6H).

BAPN treatment also led to significantly impaired function in p14BAPNd56 injured IVDs. BAPN treatment significantly reduced DHI in injured IVDs compared to untreated injured p14 IVDs that had DHI restoration (Figures 6I–6K). There were no changes due to BAPN treatment with torsional testing suggesting the robust fibrotic healing in p14BAPN mice was capable of restoring torsional properties after healing (Figures 6L and 6M). However, there was an increase in compressive stiffness (Figure 6N) in p14BAPN mice but not tensile stiffness or range of motion (Figures 6O and 6P), which combined with reduced DHI suggests the collapse and compaction of the IVD, consistent with the histological findings showing the degradation of the AF layers. Overall, BAPN treatment impaired healing compared to untreated p14 mice and shifted p14d56 IVDs from regenerative healing to fibrotic healing with loss of disc height and impaired biomechanical function. Since p14BAPN reduced collagen crosslinking density without affecting % cell proliferation, results indicate that maintaining crosslinking density and AF structure organization is essential to regenerative healing and that high % cell proliferation is not sufficient for AF regenerative healing conditions.

Bulk sequencing on AF tissue from p14 and p28 mice was used to identify additional factors likely to limit regenerative AF healing. Despite the relative closeness in age, the PCA plot revealed that p14 and p28 transcriptomes could be easily separated (Figure 7A), with 851 DEGs

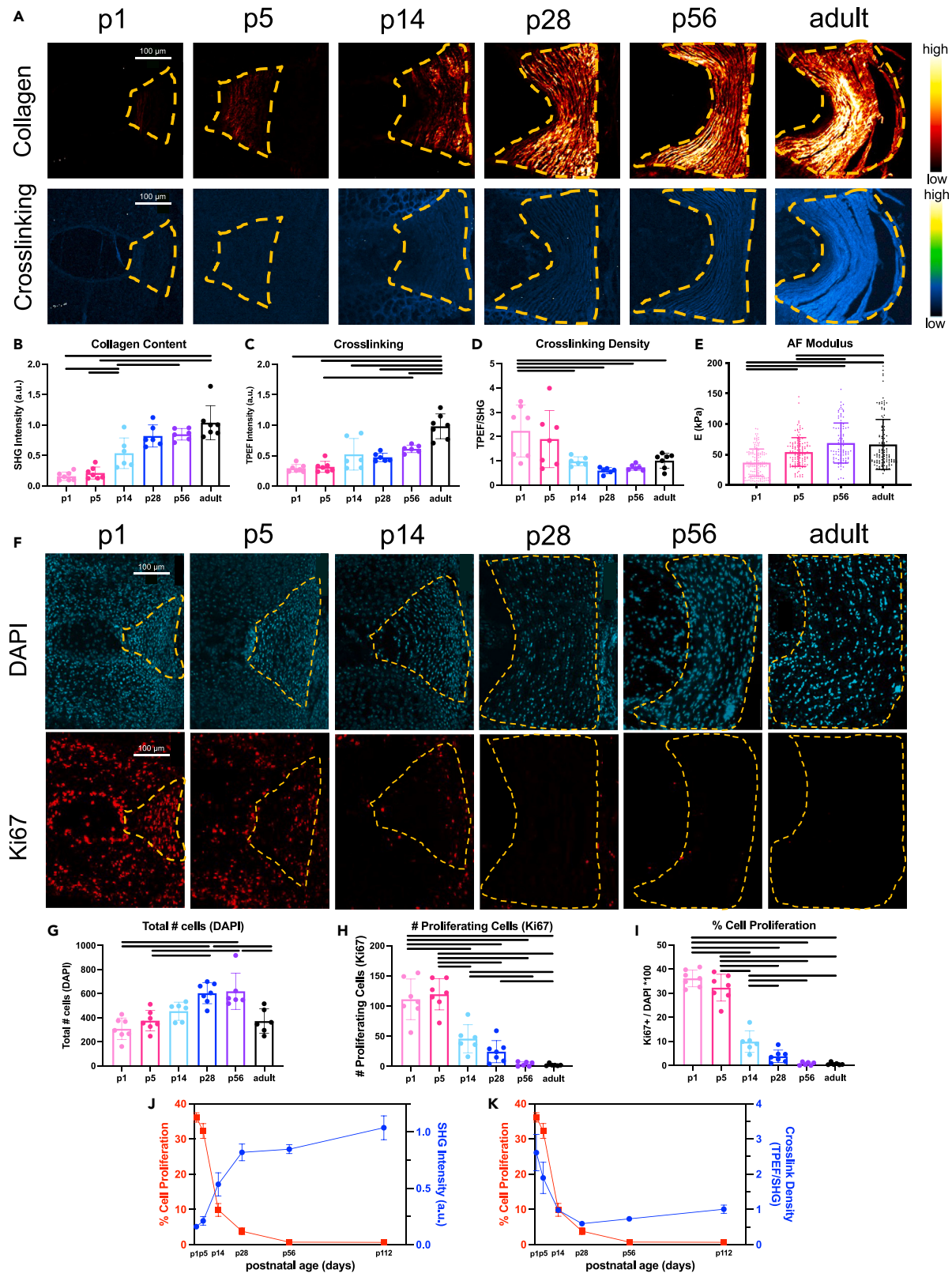
A
p1
p5
p14
p28
p56
adult
Collagen
Crosslinking
100 μm
high
low
high
low
B
Collagen Content
SHG Intensity (a.u.)
C
Crosslinking
TPEF Intensity (a.u.)
D
Crosslinking Density
TPEF/SHG
E
AF Modulus
E (kPa)
F
DAPI
Ki67
G
Total # cells (DAPI)
H
Proliferating Cells (Ki67)
I
% Cell Proliferation
Ki67+ / DAPI *100
J
% Cell Proliferation
SHG Intensity (a.u.)
postnatal age (days)
K
% Cell Proliferation
Crosslink Density (TPEF/SHG)
postnatal age (days)

Figure 4. Postnatal AF growth involves rapidly increased collagen accumulation and AF modulus with reduced crosslinking density and AF cell proliferation

(A) Representative IVD images (biological n = 6–9/age) under second harmonic generation (SHG, excitation 910 nm) depicting collagen content, and two photon excitation fluorescence (TPEF, excitation 720nm) depicting crosslinking. Scale bars = 100 μm.

(B–D) Quantification of (B) collagen content (C) crosslinking and (D) crosslinking density (TPEF/SHG).

(E) Quantification of AF elastic modulus, E.

(F–I) Representative AF images (n = 6–9/age) of DAPI and Ki67 (cell proliferation) Quantification of (G) total number of AF cells (H) number of proliferating cells, and (I) % cell proliferation.

(J) Inverse relationship between % AF cell proliferation (Ki67/DAPI) and collagen content (SHG).

(K) Proportional relationship between % AF cell proliferation (Ki67/DAPI) and crosslink density (TPEF/SHG). Error bars = SD. Effect of age was evaluated by one way ANOVA with Tukey post-hoc comparisons. $p < 0.05$ is considered significant and indicated in graphs as a horizontal black line.

between p14 and p28 AF tissue with roughly half of these genes significantly higher in the p28 and half significantly lower (Figure 7B). GSEA with Enrichr on DEGs identified GO terms for significantly depleted and enriched pathways in p28 AF cells. Importantly, top GO terms that related to the ECM structure, organization, and collagen fibril organization were depleted at p28 compared to p14, confirming the importance of AF lamellar and collagen organization in p14 regenerative mice (Figures 7C and S9), and providing an external validation that disrupted collagen crosslinking is likely to be a key factor limiting regenerative healing in p14-BAPN animals. The p28 AF tissue also revealed top GO terms enriched for immune related responses including neutrophil degranulation, neutrophil activation, and cellular response to cytokine stimulus (Figures 7C and S9). The importance of immune cell responses in other neonatal tissues motivated us to characterize immune cell differences from p14d56 to p28d56 using immunohistochemical staining against CD45, a pan immune-cell marker found on all leukocytes (Figure 7D). Interestingly, CD45 staining was most prominent in p14d56 IVDs with an abundance of positively stained cells in the newly deposited repair tissue in the injury sites of p14d56 IVDs and beyond the boundary of the native AF (Figures 7E and 7F). There was no positive CD45 staining in the fibrous cap of p28d56 mice IVDs, and no CD45 staining within the injury site which did not contain any cells or repair tissue. The $CD45^{+}$ cells were quantified (Figure 7E) to be significantly higher grades for p14d56 compared to p28d56 (Figure 7F). Additional bulk sequencing performed on p5 and p21 AF tissue revealed distinct gene expression profiles for p5, p14, and p28 mice. p21 had more variance between samples and were intermixed with p14 and p28 samples suggesting p21 has overlap with the two closest ages (Figure S10).

DISCUSSION

This IVD regeneration study applied AF herniation injuries to neonatal mice to answer important open questions in IVD regeneration and to identify necessary factors for AF regenerative healing. IVDs healed regeneratively when these large-sized injuries were induced at very early neonatal ages from p1 through p14 and transitioned to fibrotic healing when injured at p28. Healing was considered functionally regenerative since it involved cellular repair tissue with organized collagen within the IVD space, retained AF lamellar structure adjacent to the injury, restored IVD height, and restored biomechanical function. However, injured mice IVDs did not recapitulate the native AF lamellar structure even when injured at p1, which contrasts regenerative healing in other organs and tissues with comparably large-sized injuries. Our growth study determined this period when the "window of regenerative healing closes" coincides with a shift in the expansive neonatal IVD growth from rapid cell proliferation to extensive collagen deposition. The substantially altered collagen crosslinking density after p14 implicated its role in regenerative healing. We therefore pharmacologically decreased AF crosslinking by inhibiting lysyl oxidase with BAPN which reduced collagen crosslinking without affecting cell proliferation. BAPN treatment shifted AF healing from regenerative to fibrotic highlighting the necessity of high crosslink density to stabilize AF layers during healing processes and underscoring that high cell mitotic rates are not sufficient for regeneration. Bulk RNA-seq of p14 (regenerative healing age) and p28 (fibrotic healing age) AF tissues revealed GO terms for depleted extracellular matrix organization processes at p28 providing an unbiased validation that crosslinking is a key change at the age when the IVD regenerative healing window closes. RNA-seq also identified upregulated GO terms for neutrophil degranulation at p28 implicating immune cell changes in the shift to fibrosis, which was further supported by stark differences in immune cell presence in AF repair tissue from regenerative p14 to fibrotic p28 IVDs. This mouse model identified a novel temporal window in which to study cellular and molecular processes involved in the limited regenerative potential of the adult mammalian IVD, and determined that design criteria for human AF repair methods include retained AF lamellar integrity in proximity to injury sites and delivery or recruitment of cells with mitotic potential capable of depositing matrix to restore IVD height and biomechanical function.

IVD regenerative healing did not recapitulate the native AF structure at any neonatal age in this model and we believe this is likely related to loading conditions on the IVD caused by this herniation injury, although it is important to also contextualize our findings with injury-size effects. This study applied injuries with AF puncture ~80% IVD height through ~50% IVD width to induce NP herniation, and this large and "criticallysized" injury was selected to cause IVD injuries shown to cause progressive IVD degeneration in adult mice and with detectable IVD biomechanical changes that are easier to detect than smaller injuries that do not consistently induce detectable biomechanical changes.[23,24] Injury size effects were similarly demonstrated in neonatal cardiac healing since controlled amputation of <15% of the myocardial tissue was regenerative with structural restoration, while larger injuries did not regenerate at any age.[25] Interestingly, complete tendon transection in neonatal mice (i.e., considered more severe than the IVD herniation injury here), was capable of structural and functional regeneration,[10] and we speculate this is because there is no compressive damage to the tendon from loading after the injury. We further believe our injury was "critically-sized" and unable to recapitulate its structure since the loss of NP pressurization during herniation injury can result in repetitive AF damage with lamellar buckling, loss of AF collagen fiber tension and progressive damage, AF cell apoptosis and matrix

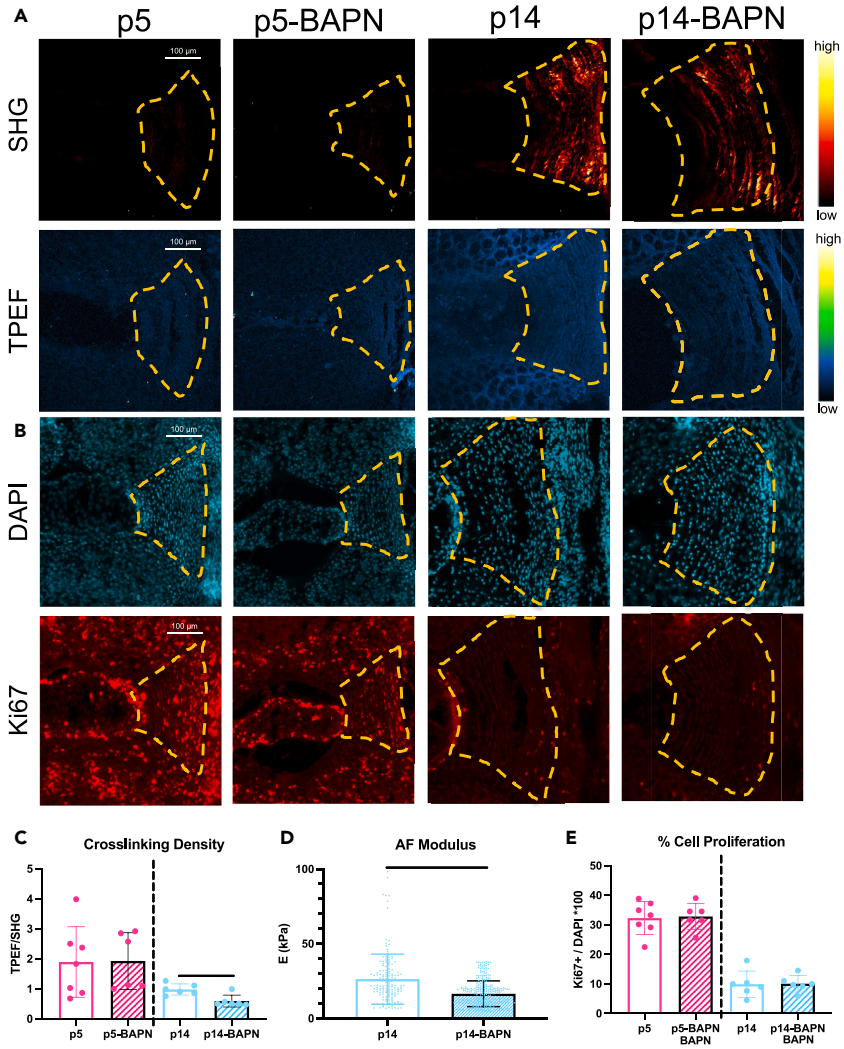

Figure 5. Inhibiting crosslinking accumulation with BAPN reduced AF crosslinking density and modulus at p14 without affecting % cell proliferation

BAPN was administered through drinking water until embryonic day 5.5 until p5 or p14 (biological n = 6–9/age).

(A and B) Representative (A) multiphoton images of SHG (collagen content) and TPEF (collagen crosslinking) and (B) fluorescent images of total cells (DAPI) and proliferating cells (Ki67) in control and BAPN-treated p5 and p14 AF tissue. Scale bars = 100 μm.

(C–E) Quantification of (C) collagen crosslinking density (TPEF/SHG) (D) AF tissue elastic modulus, and (E) % cell proliferation.

Dashed lines outline AF region (yellow). Error bars = SD. Student's t test with $p < 0.05$ determined significance, depicted in graphs as a horizontal black line. p5 and p14 mice were the same as in the growth studies as all groups were processed and analyzed together.

catabolism.[26,27] Needle size was adjusted to account for IVD size changes during growth (Figure S1C), and we believe was sufficiently controlled to enable us to sufficiently conclude the shift from regenerative to fibrotic healing occurred from p14 to p28. Mouse and human lumbar IVDs have many similarities in IVD structure and biomechanical stress environments when normalized for geometric differences, and we therefore expect biomechanical factors to be similar across species.[28,29] Coccygeal IVDs provide easy access to surgical injury interventions as in this study, while also retaining structural and biomechanical similarities to the lumbar spine including supporting significant axial stresses due to muscular loading (since muscle loading dominates gravitational loading in prescribing axial loads in all spinal regions of humans and quadrupeds).[30,31] Therefore herniation injury can similarly result in repetitive AF damage in IVDs of all spinal levels and species including mouse coccygeal IVDs in this study. Partial and full depth AF puncture injuries in adult murine IVDs from lumbar and coccygeal regions reported that full-depth (i.e., complete) AF injuries caused significant degeneration throughout the entire IVD while the partial-depth (i.e., that retained NP pressure) AF injuries caused only localized disruptions mainly contained to the AF.[32,33] We expect a partial-depth AF injury or small needle puncture in neonates that retains NP pressure and may be capable of full structural regeneration since the AF would not be subjected to subsequent compressive damage. Nevertheless, critically-sized IVD herniation injury is the more important clinical challenge, and in this study, neonates up to p14 healed remarkably well and we call it regenerative and/or functional regeneration.

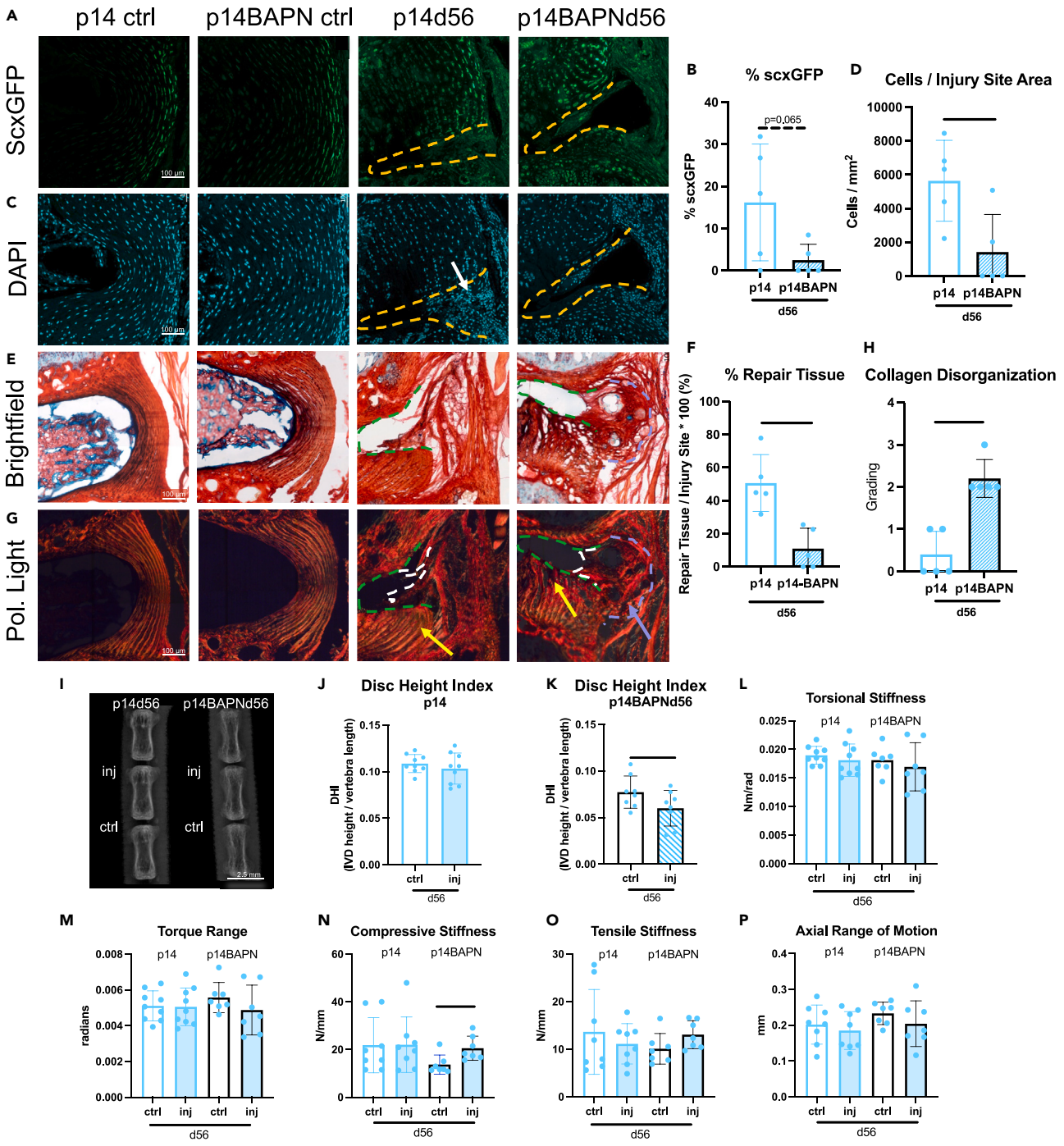

Figure 6. BAPN treatment shifted p14 regenerative healing to fibrotic healing with little matrix/cell deposition, fibrotic caps, reduced DHI, and increased compressive stiffness

BAPN-treated mice were injured at p14 and evaluated 56 days after injury (n = 5).

(A–H) Representative fluorescent images of (A) *ScxGFP* (AF cells) and (B) DAPI (total number of cells) are used to quantify (C) cells/injury site area and (D) % with *ScxGFP*. Representative PRAB (E) brightfield and (F) polarized light images are used to quantify (G) % Repair Tissue and (H) Collagen Disorganization grade. Scale bars = 100 µm. Dashed lines outlines injury sites (yellow or green), fibrous caps (purple), and repair tissue (white). Arrows point toward cellular repair tissue (white), fibrous caps (purple), and adjacent AF structures near injury sites (yellow).

(I) Digital X-rays were used to calculate DHI in (J) p14 and (K) p14BAPN mice 56 days after injury (biological n = 6–9/age).

Torsional (L and M) and (N and P) axial biomechanical parameters. Error bars = SD. Student's t test with $p < 0.05$ determined significance, depicted in graphs as a horizontal black line. p14d56 mice were the same as in the regeneration window studies as all groups were processed and analyzed together.

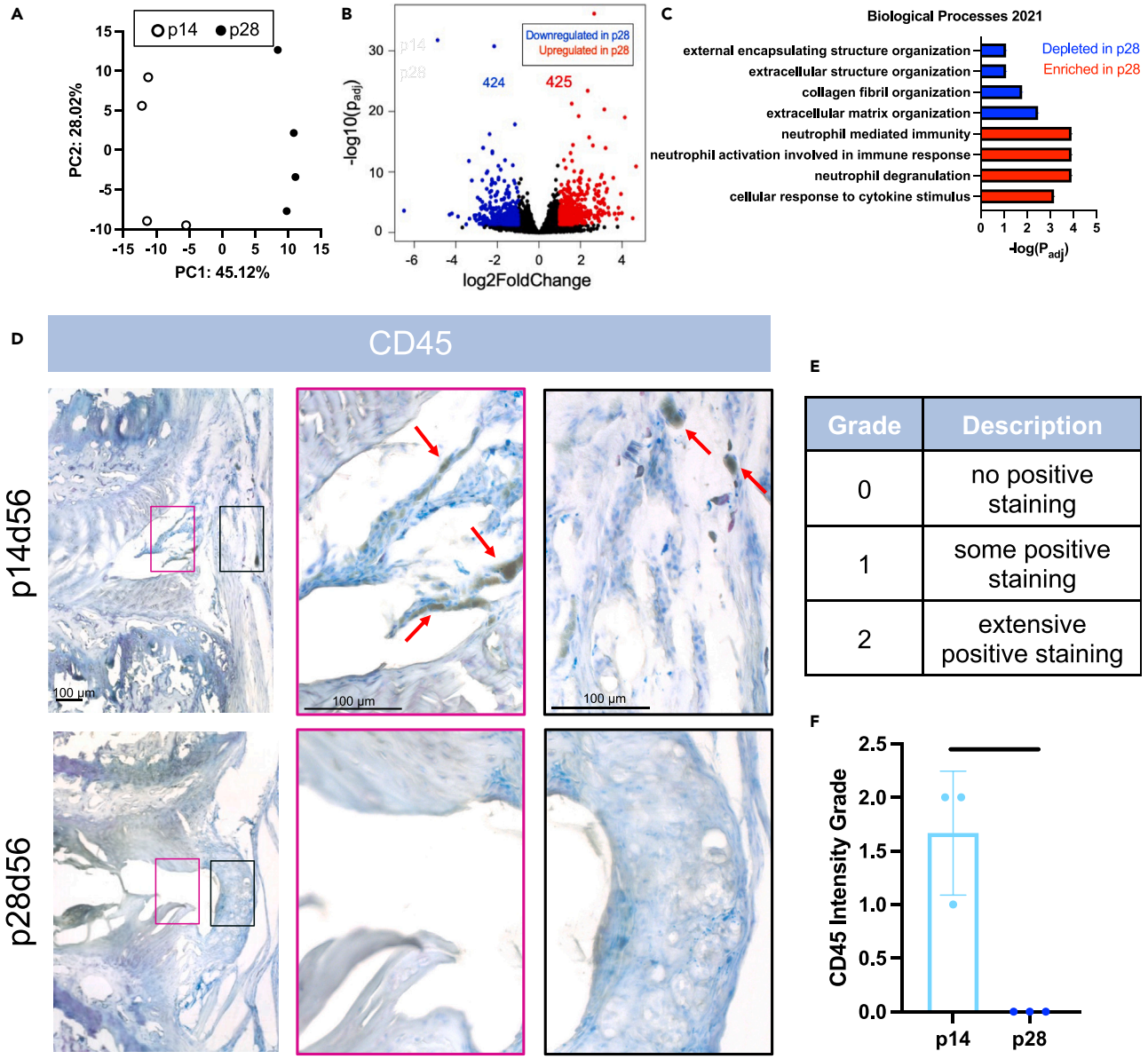

Figure 7. p28 AF has depleted structural organization pathways, enriched immune-related pathways, and fewer CD45-immune cells at the injury site compared to p14

(A–C) Bulk sequencing of p14 and p28 AF tissue (n = 4 samples/age) revealed (A) PCA plot highlighting p14 and p28 gene expression profiles are distinct with (B) volcano plot depicting the number of differentially expressed genes (DEGs) and (C) GO-Terms found using Enrichr highlighting the most significant enriched and depleted pathways.

(D) Immunohistochemical staining of leukocyte cell marker CD45 using a peroxidase/DAB secondary kit with a TOL Blue counterstain on p14 and p28 IVDs (n = 3/age) 56 days after injury. Arrows (red) point toward representative positive cells (black). Pink and black insets highlight areas within injury sites within the boundary of the IVD (pink) and on the outer periphery (black).

(E) Scale bars = 100 µm (E) $CD45^+$ staining semi-quantification grading scale.

(F) $CD45^+$ grading for p14 and p28 IVDs 56 days after injury. Error bars = SD. Student's t test with $p < 0.05$ determined significance, depicted in graphs as a horizontal black line.

Regenerative AF healing up to p14 shifted to fibrotic healing by p28 which expands and refines prior knowledge. Specifically, regenerative AF healing in p1, p5, and p14 in this study was similar to functional regenerative IVD healing previously reported in p5 mice IVDs.[11] This study further clarified AF regenerative healing involves highly cellular repair tissue with organized collagen, retained AF layers adjacent to the injury site, and restored IVD height and biomechanical properties. In contrast, fibrotic healing in mice injured at p28 involves little/no repair tissue in the injury defect site, degeneration of AF layers adjacent to the injury site, a fibrous "cap" on the periphery of the IVD populated by fibroblastic

cells with disorganized (i.e., little birefringence in polarized light imaging) collagen, IVD height loss, and altered biomechanical function. Fibrotic healing in this study was consistent with broader IVD literature documenting mature IVDs heal with a fibrous cap consisting of mature fibroblasts and collagens which form on the periphery and can extend inwards in IVDs from rabbits and mice.[11,34] The p28 mice have a human equivalent age of approximately 10–15 years, and the lack of robust regenerative healing when IVDs are injured at such young ages suggests a reason why some morphological and compositional changes in the human IVDs can be considered degenerative even when occurring at very young ages.[1] Human NP cells shift from notochordal to non-notochordal phenotype by 10 years which is a similar age and often speculated to be a cause of premature IVD degeneration.[35–37] However, the notochordal cell transition is unlikely to be a factor in the shift to fibrotic healing observed in this study since the notochordal NP cell phenotype persists in mice beyond 9 months, and since fibrotic AF healing has been observed in multiple species including notochordal-cell retaining and non-notochordal IVD models.[34,35,38,39] The shift to fibrosis at such early ages therefore implicates the changes in IVD cell proliferation and matrix structure occurring during this explosive IVD growth period in mice from p1 to p14 and to p28.

Our growth study identified a shift in growth mechanisms from high cell proliferation rates to extensive collagen deposition that coincided with postnatal ages where regenerative healing shifts to fibrosis. This study expands on the IVD growth literature to show that neonatal AF growth involves lamellar collagen structural deposition with increasing birefringence most prominent on polarized light around p14. This expansive growth stage involves organized collagen deposition that outpaces crosslinking accumulation to result in significantly decreased crosslinking density (Figure 4). RNA-seq confirmed the importance of structural changes during this growth stage since GSEA identified depleted GO terms for structure organization, collagen fibril organization, and extracellular matrix organization. Since AF layers are created during development and the number of AF layers are nearly constant in the mice postnatally, we do not expect the number of AF layers to play a role in the shift from regenerative to fibrotic AF healing.[12,13] Therefore, this growth study and the literature implicated reduced cell mitosis and crosslinking density as two potential factors with significant changes at p14 that are likely to affect AF regenerative potential.

The highly cellular AF repair tissue in regenerative healing implicated high cell proliferation rates as being permissive of AF regenerative healing, yet this study showed high AF cell mitosis is not sufficient for regenerative healing. A previous lineage tracing showed regenerative AF healing in injured p5 IVDs involved Scx-lineage cells that de-differentiated following injury, adopted a stem-like (Sca-1+) phenotype, proliferated to expand cell number, and then re-differentiated toward type 1 collagen producing *ScxGFP+* AF cells by d56.[40] Because of the expected importance of AF cell mitotic potential in AF regeneration, we measured AF cell proliferation rates with high timing resolution and with 2 different methods, Ki67 IHC in the AF (Figure 5) and Edu in AF, NP and cartilage endplate regions (Figures S6 and S7). The ages when IVD cells had reduced proliferation rates were consistent between methods and with prior literature showing undetectable cell proliferation rates in mouse lumbar spine by 28 days.[12] Importantly, this study determined high rates of AF cell proliferation were not sufficient for AF regenerative healing based on three findings. First, AF herniation injury healed similarly at p5 and p14 despite the lower levels of proliferating AF cells in p14. Second, BAPN-treated mice had inferior AF healing, but the treatment did not affect cell proliferation rates. Third, unbiased RNA-seq analysis between p14 and p28 AF did not detect significant GO terms relating to cell cycle or proliferation changes, suggesting the significant decreases in Ki67 and Edu are less dominant than other changes detected. AF tissue regeneration therefore appears to be independent of cell mitosis levels, consistent with the neonatal heart which loses its regenerative potential at p2 (with fibrous scarring when injured at p2 and healing without scars when injured at p1) even though most cardiomyocytes become post-mitotic at p5.[15,41] Nevertheless, it is somewhat likely that high AF cell proliferation rates are a necessary condition for AF regenerative healing which remains a future question since cells expressing Scx and Mhk are important in AF repair, and identifying AF progenitors with enhanced appreciation for the complexity of AF cell populations remains an evolving research topic with several recent single-cell RNA-seq analyses.[42–44]

This study showed that maintaining AF lamellar AF matrix microenvironment conditions was necessary for IVD regenerative healing. Specifically, inferior IVD healing with BAPN treatment in this study provided direct evidence that AF's high crosslinking density with organized collagen structure was a necessary condition for AF regenerative healing. AF injury in p14 mice treated with BAPN had fibrotic healing, degenerated surrounding AF tissues, and loss of IVD height. BAPN treatment in p14 mice decreased AF crosslinking without affecting AF cell proliferation, IVD width, or vertebral growth, further suggesting these changes are related to altered crosslinking density. While the growth study implicated changes in collagen content and crosslinking density in the shift to fibrotic healing, we note that BAPN did not affect collagen content (Figure 5C) and therefore crosslink density changes are most likely to have affected inferior IVD healing with BAPN treatment. We believe decreased crosslinking from BAPN made IVDs more susceptible to matrix degradation and progressive damage during acute inflammation occurring at early healing stages.[45] Increased matrix degradation in the injured p14 with BAPN animals is consistent with the observed loss of IVD height and increased biomechanical compressive stiffness, which may result from increased IVD deflections and endplate contact under load. RNA-seq was an unbiased confirmation of the importance of collagen structural changes in the shift to fibrotic healing since GSEA revealed top GO terms for extracellular organization, collagen fibril organization, and extracellular structure organization when comparing non-regenerative (p28) to regenerative (p14) AF tissue. We believe that an organized AF matrix contains refined structural features, such as microtubules,[46,47] that may facilitate the transport of cells and soluble factors that better enable healing.

BAPN treatment rescued cardiac regenerative capacity in neonatal mice yet caused inferior IVD healing in this study.[15] Cell culture studies show lower substrate stiffness and increased access to cell-adhesive ligands can increase proliferation rates and enhance stemness in different cells.[48–50] We therefore expected BAPN to improve IVD healing since BAPN would reduce AF tissue modulus, and enhance cell proliferation and transport. However, BAPN caused fibrotic IVD healing in p14 mice by reducing crosslinking density without affecting IVD cell proliferation. We believe the differences in cardiac and IVD loading conditions may explain why BAPN improved healing in neonatal cardiac and diminished healing in IVDs. Cardiac tissues are loaded in tension biaxially while the AF is loaded in tension circumferentially (from hoop

stresses) and compression axially.[51,52] Axial IVD compression causes complex AF strain patterns that can cause lamellar buckling and delamination which induces apoptosis and promotes catabolism.[27,53] We believe that BAPN impaired IVD healing is due to local IVD effects with the accumulation of collagen disorganization due to weakened AF collagen because BAPN-treated animals had normal weight and health. Furthermore, systemic BAPN effects are unlikely to reach a threshold to influence the IVDs of the young treated mice in this study (e.g., tendon changes to increase joint motion are unlikely to substantially influence the large range of motion of healthy coccygeal IVD motion segments[16]; and reduced blood pressure is unlikely to significantly impair IVD nutrition in these small young coccygeal mouse IVDs[54]). Additionally, loss of AF residual strains from IVD puncture can cause apoptosis, fibrous scarring, and aberrant mechanosensing.[26] BAPN-induced crosslink reduction therefore seems to impact healing differently in tissues experiencing distinct loading conditions. This study together with the literature therefore strongly emphasizes the importance of crosslinking with retained AF structure for IVD homeostasis and healing. AF repair strategies informed by this study would therefore need to consider the stabilization of native AF lamellae adjacent to the injury sites which may arrest progressive degeneration and be sufficient to enable functional healing without the need to fully recapitulate native AF and NP structures. For example, a cell-seeded AF sealant stabilized AF layers adjacent to the injury site in bovine organ culture, while unrepaired defects underwent progressive degeneration of adjacent AF layers.[55]

This study implicated a role for immune cell changes in the transition from regenerative to fibrotic IVD healing since GSEA from p14 to p28 AF tissue revealed top GO terms enriched for neutrophil degranulation and neutrophil activation. Meanwhile, immunostaining showed more CD45 staining in p14d56 than in p28d56, suggesting a different and more robust inflammatory response in regenerative vs. fibrotic healing. Regenerative healing in neonatal mouse tendons also involved a more robust immune response influenced by macrophages with neonatal Tregs controlling macrophage polarization, compared to a more chronic and less robust immune response in adult tendon fibrotic healing.[56,57] Regeneration in neonatal mouse cardiac tissue and salamander cardiac tissue have been shown to require macrophages, with loss of regenerative ability after macrophage depletion.[58,59] Puncture injury in adult rat IVDs was shown by single-cell RNA-seq to involve macrophages and B lymphocytes[60] while the systemic ablation of macrophages led to increased IVD herniation size, further suggesting immune cell involvement in altered IVD healing patterns.[61] Our results in the context of the literature, therefore, highlight a more robust inflammatory response in regenerative healing, and a need for future studies to identify the immune cells involved in neonatal IVD regeneration.

In conclusion, this study identified that matrix changes occurring between p14 and p28 are critical drivers in the transition from functional regeneration to fibrotic IVD healing while high AF cell proliferation rates were not sufficient to enable regenerative healing. However, the IVD lamellar structure was not fully recapitulated following injury at any neonatal age contrasting other neonatal tissues with similar injury severity, likely because IVD herniation injury caused loss of AF fiber tension with repetitive compressive damage. High collagen crosslink density and maintained lamellar organization were necessary conditions for IVD functional regeneration, which may be critical in avoiding compressive lamellar damage and retaining AF microstructural features that are permissive to transporting cells and soluble factors. Translating these concepts suggests design goals for IVD regenerative repair would retain AF lamellar integrity in proximity to injury sites while delivering or recruiting cells capable of depositing matrix to restore AF tension, IVD height, and biomechanical function in order to limit and avoid compressive damage to AF lamellae.

Limitations of the study

Inhibited crosslink density shifted IVD healing from regenerative to fibrotic healing, yet we did not add crosslinks to the IVD to try a "rescue" experiment since crosslinking agents have known cytotoxicity and are nearly impossible to localize precisely to the AF defect site in very small mouse IVDs. Bulk RNA-seq was used as an unbiased validation of the importance of AF matrix organization at ages when IVDs shift from regenerative to fibrotic healing, and the immune cell changes also identified are presented as descriptive findings to inspire future work. AF elastic modulus calculated with AFM nanoindentation was not comparable between the aging study (p1, p5, p56, and adults) and the BAPN study (p14 and p14-BAPN) since the AFM probe used in the first study was discontinued by the vendor and the replacement probe for the second study had a small bias when comparing across the sub-studies. Additionally, throughout the study, we used uninjured adjacent IVDs as internal controls to minimize variability between individual mice and to reduce the number of mice required. Utilizing uninjured adjacent controls rather than separate uninjured mice can be a limitation, but we did not detect any suggestion of adjacent segment degeneration in the internal control IVDs.

RESOURCE AVAILABILITY

Lead contact

Further information and requests for resources and reagents should be directed to and will be fulfilled by the lead contact, James Iatridis (james.iatridis@mssm.edu).

Materials availability

This study did not generate new unique reagents.

Data and code availability

- The bulk RNA-seq dataset generated in this study is publicly available at Gene Expression Omnibus (GEO: GSE275620).
- This article does not report the original code.
- Any additional information required to reanalyze the data reported in this article is available from the lead contact upon request.

ACKNOWLEDGMENTS

Funded by National Institute of Health NIH/NIAMS grants R01AR080096 and R01AR078857. Multiphoton microscope (NIH S10RR026639) in Microscopy CoRE at Mount Sinai. AFM (NIH S10 RR027609) in cardiovascular AFM Core. The authors gratefully acknowledge Dr. Ronen Schweitzer (Shriners Children Hospital, Portland, OR) for *ScxGFP* mice, and Ms. Victoria Mroz for assistance on Edu quantification.

AUTHOR CONTRIBUTIONS

Conceptualization: DND, AHH, and JCI, methodology: DND, KA, AMR, RJW, OMT, EDF, and PN, investigation: DND, KA, AMR, RJW, OMT, EDF, and PN, visualization: DND, supervision: KDC, WMH, AHH, and JCI, writing—original draft: DND and JCI, writing—review and editing: DND, KA, AMR, RJW, PN, OMT, EDF, KDC, WMH, AHH, and JCI.

DECLARATION OF INTERESTS

The authors declare no competing interests.

STAR★METHODS

Detailed methods are provided in the online version of this paper and include the following:

SUPPLEMENTAL INFORMATION

Supplemental information can be found online at https://doi.org/10.1016/j.isci.2024.110883.

Received: June 5, 2024
Revised: August 18, 2024
Accepted: September 2, 2024
Published: September 4, 2024

REFERENCES

1. Adams, M.A., and Roughley, P.J. (2006). What is intervertebral disc degeneration, and what causes it? Spine *31*, 2151–2161. https://doi.org/10.1097/01.brs.0000231761.73859.2c.
2. Mohanty, S., and Dahia, C.L. (2019). Defects in intervertebral disc and spine during development, degeneration, and pain: New research directions for disc regeneration and therapy. Wiley Interdiscip. Rev. Dev. Biol. *8*, e343. https://doi.org/10.1002/wdev.343.
3. Hartvigsen, J., Hancock, M.J., Kongsted, A., Louw, Q., Ferreira, M.L., Genevay, S., Hoy, D., Karppinen, J., Pransky, G., Sieper, J., et al. (2018). What low back pain is and why we need to pay attention. Lancet *391*, 2356–2367. https://doi.org/10.1016/S0140-6736(18)30480-X.
4. Dieleman, J.L., Cao, J., Chapin, A., Chen, C., Li, Z., Liu, A., Horst, C., Kaldjian, A., Matyasz, T., Scott, K.W., et al. (2020). US Health Care Spending by Payer and Health Condition, 1996-2016. JAMA *323*, 863–884. https://doi.org/10.1001/jama.2020.0734.
5. Iatridis, J.C., Nicoll, S.B., Michalek, A.J., Walter, B.A., and Gupta, M.S. (2013). Role of biomechanics in intervertebral disc degeneration and regenerative therapies: what needs repairing in the disc and what are promising biomaterials for its repair? Spine J. *13*, 243–262. https://doi.org/10.1016/j.spinee.2012.12.002.
6. Sloan, S.R., Lintz, M., Hussain, I., Hartl, R., and Bonassar, L.J. (2018). Biologic annulus fibrosus repair: A review of preclinical in vivo investigations. Tissue Eng. Part B *24*, 179–190. https://doi.org/10.1089/ten.TEB.2017.0351.
7. Kirnaz, S., Singh, S., Capadona, C., Lintz, M., Goldberg, J.L., McGrath, L.B., Medary, B., Sommer, F., Bonassar, L.J., and Härtl, R. (2022). Innovative biological treatment methods for degenerative disc disease. World Neurosurg. *157*, 282–299. https://doi.org/10.1016/j.wneu.2021.09.068.
8. Panebianco, C.J., Constant, C., Vernengo, A.J., Nehrbass, D., Gehweiler, D., DiStefano, T.J., Martin, J., Alpert, D.J., Chaudhary, S.B., Hecht, A.C., et al. (2023). Combining adhesive and nonadhesive injectable hydrogels for intervertebral disc repair in an ovine discectomy model. JOR Spine *6*, e1293. https://doi.org/10.1002/jsp2.1293.
9. Porrello, E.R., Mahmoud, A.I., Simpson, E., Hill, J.A., Richardson, J.A., Olson, E.N., and Sadek, H.A. (2011). Transient regenerative potential of the neonatal mouse heart. Science *331*, 1078–1080. https://doi.org/10.1126/science.1200708.
10. Howell, K., Chien, C., Bell, R., Laudier, D., Tufa, S.F., Keene, D.R., Andarawis-Puri, N., and Huang, A.H. (2017). Novel model of tendon regeneration reveals distinct cell mechanisms underlying regenerative and fibrotic tendon healing. Sci. Rep. *7*, 45238. https://doi.org/10.1038/srep45238.
11. Torre, O.M., Das, R., Berenblum, R.E., Huang, A.H., and Iatridis, J.C. (2018). Neonatal mouse intervertebral discs heal with restored function following herniation injury. FASEB J. *32*, 4753–4762. https://doi.org/10.1096/fj.201701492R.
12. Dahia, C.L., Mahoney, E.J., Durrani, A.A., and Wylie, C. (2009). Postnatal growth, differentiation, and aging of the mouse intervertebral disc. Spine *34*, 447–455. https://doi.org/10.1097/BRS.0b013e3181990c64.
13. Leung, V.Y.L., Chan, W.C.W., Hung, S.-C., Cheung, K.M.C., and Chan, D. (2009). Matrix remodeling during intervertebral disc growth and degeneration detected by multichromatic FAST staining. J. Histochem. Cytochem. *57*, 249–256. https://doi.org/10.1369/jhc.2008.952184.

14. Antoniou, J., Steffen, T., Nelson, F., Winterbottom, N., Hollander, A.P., Poole, R.A., Aebi, M., and Alini, M. (1996). The human lumbar intervertebral disc: evidence for changes in the biosynthesis and denaturation of the extracellular matrix with growth, maturation, ageing, and degeneration. J. Clin. Invest. *98*, 996–1003. https://doi.org/10.1172/JCI118884.
15. Notari, M., Ventura-Rubio, A., Bedford-Guaus, S.J., Jorba, I., Mulero, L., Navajas, D., Martí, M., and Raya, Á. (2018). The local microenvironment limits the regenerative potential of the mouse neonatal heart. Sci. Adv. *4*, eaao5553. https://doi.org/10.1126/sciadv.aao5553.
16. Marturano, J.E., Arena, J.D., Schiller, Z.A., Georgakoudi, I., and Kuo, C.K. (2013). Characterization of mechanical and biochemical properties of developing embryonic tendon. Proc. Natl. Acad. Sci. USA *110*, 6370–6375. https://doi.org/10.1073/pnas.1300135110.
17. Marturano, J.E., Xylas, J.F., Sridharan, G.V., Georgakoudi, I., and Kuo, C.K. (2014). Lysyl oxidase-mediated collagen crosslinks may be assessed as markers of functional properties of tendon tissue formation. Acta Biomater. *10*, 1370–1379. https://doi.org/10.1016/j.actbio.2013.11.024.
18. Handorf, A.M., Zhou, Y., Halanski, M.A., and Li, W.-J. (2015). Tissue stiffness dictates development, homeostasis, and disease progression. Organogenesis *11*, 1–15. https://doi.org/10.1080/15476278.2015.1019687.
19. Wells, R.G. (2008). The role of matrix stiffness in regulating cell behavior. Hepatology *47*, 1394–1400. https://doi.org/10.1002/hep.22193.
20. Pryce, B.A., Brent, A.E., Murchison, N.D., Tabin, C.J., and Schweitzer, R. (2007). Generation of transgenic tendon reporters, ScxGFP and ScxAP, using regulatory elements of the scleraxis gene. Dev. Dynam. *236*, 1677–1682. https://doi.org/10.1002/dvdy.21179.
21. Masuda, K., Aota, Y., Muehleman, C., Imai, Y., Okuma, M., Thonar, E.J., Andersson, G.B., and An, H.S. (2005). A novel rabbit model of mild, reproducible disc degeneration by an anulus needle puncture: correlation between the degree of disc injury and radiological and histological appearances of disc degeneration. Spine *30*, 5–14. https://doi.org/10.1097/01.brs.0000148152.04401.20.
22. Wang, D., Lai, A., Gansau, J., Seifert, A.C., Munitz, J., Zaheer, K., Bhadouria, N., Lee, Y., Nasser, P., Laudier, D.M., et al. (2023). Lumbar endplate microfracture injury induces Modic-like changes, intervertebral disc degeneration and spinal cord sensitization - an in vivo rat model. Spine J. *23*, 1375–1388. https://doi.org/10.1016/j.spinee.2023.04.012.
23. Martin, J.T., Gorth, D.J., Beattie, E.E., Harfe, B.D., Smith, L.J., and Elliott, D.M. (2013). Needle puncture injury causes acute and long-term mechanical deficiency in a mouse model of intervertebral disc degeneration. J. Orthop. Res. *31*, 1276–1282. https://doi.org/10.1002/jor.22355.
24. Elliott, D.M., Yerramalli, C.S., Beckstein, J.C., Boxberger, J.I., Johannessen, W., and Vresilovic, E.J. (2008). The effect of relative needle diameter in puncture and sham injection animal models of degeneration. Spine *33*, 588–596. https://doi.org/10.1097/BRS.0b013e318166e0a2.
25. Bryant, D.M., O'Meara, C.C., Ho, N.N., Gannon, J., Cai, L., and Lee, R.T. (2015). A systematic analysis of neonatal mouse heart regeneration after apical resection. J. Mol. Cell. Cardiol. *79*, 315–318. https://doi.org/10.1016/j.yjmcc.2014.12.011.
26. Bonnevie, E.D., Gullbrand, S.E., Ashinsky, B.G., Tsinman, T.K., Elliott, D.M., Chao, P.-H.G., Smith, H.E., and Mauck, R.L. (2019). Aberrant mechanosensing in injured intervertebral discs as a result of boundary-constraint disruption and residual-strain loss. Nat. Biomed. Eng. *3*, 998–1008. https://doi.org/10.1038/s41551-019-0458-4.
27. Walter, B.A., Korecki, C.L., Purmessur, D., Roughley, P.J., Michalek, A.J., and Iatridis, J.C. (2011). Complex loading affects intervertebral disc mechanics and biology. Osteoarthritis Cartilage *19*, 1011–1018. https://doi.org/10.1016/j.joca.2011.04.005.
28. Elliott, D.M., and Sarver, J.J. (2004). Young Investigator Award Winner: Validation of the Mouse and Rat Disc as Mechanical Models of the Human Lumbar Disc. Spine *29*, 713–722. https://doi.org/10.1097/01.BRS.0000116982.19331.EA.
29. O'Connell, G.D., Vresilovic, E.J., and Elliott, D.M. (2007). Comparison of animals used in disc research to human lumbar disc geometry. Spine *32*, 328–333. https://doi.org/10.1097/01.brs.0000253961.40910.c1.
30. Elliott, D.M., and Sarver, J.J. (2004). Young investigator award winner: validation of the mouse and rat disc as mechanical models of the human lumbar disc. Spine *29*, 713–722. https://doi.org/10.1097/01.brs.0000116982.19331.ea.
31. Smit, T.H. (2002). The use of a quadruped as an in vivo model for the study of the spine - biomechanical considerations. Eur. Spine J. *11*, 137–144. https://doi.org/10.1007/s005860100346.
32. Walk, R.E., Moon, H.J., Tang, S.Y., and Gupta, M.C. (2022). Contrast-enhanced microCT evaluation of degeneration following partial and full width injuries to the mouse lumbar intervertebral disc. Sci. Rep. *12*, 15555. https://doi.org/10.1038/s41598-022-19487-9.
33. Lai, A., Moon, A., Purmessur, D., Skovrlj, B., Laudier, D.M., Winkelstein, B.A., Cho, S.K., Hecht, A.C., and Iatridis, J.C. (2016). Annular puncture with tumor necrosis factor-alpha injection enhances painful behavior with disc degeneration in vivo. Spine J. *16*, 420–431. https://doi.org/10.1016/j.spinee.2015.11.019.
34. Smith, J.W., and Walmsley, R. (1951). Experimental incision of the intervertebral disc. J. Bone Joint Surg. Br. *33–B*, 612–625. https://doi.org/10.1302/0301-620X.33B4.612.
35. Bach, F.C., Poramba-Liyanage, D.W., Riemers, F.M., Guicheux, J., Camus, A., Iatridis, J.C., Chan, D., Ito, K., Le Maitre, C.L., and Tryfonidou, M.A. (2021). Notochordal Cell-Based Treatment Strategies and Their Potential in Intervertebral Disc Regeneration. Front. Cell Dev. Biol. *9*, 780749. https://doi.org/10.3389/fcell.2021.780749.
36. Oegema, T.R. (2002). The role of disc cell heterogeneity in determining disc biochemistry: a speculation. Biochem. Soc. Trans. *30*, 839–844. https://doi.org/10.1042/bst0300839.
37. Hunter, C.J., Matyas, J.R., and Duncan, N.A. (2004). Cytomorphology of notochordal and chondrocytic cells from the nucleus pulposus: a species comparison. J. Anat. *205*, 357–362. https://doi.org/10.1111/j.0021-8782.2004.00352.x.
38. Key, J.A., and Ford, L.T. (1948). Experimental intervertebral-disc lesions. J. Bone Joint Surg. Am. *30A*, 621–630.
39. Hampton, D., Laros, G., McCarron, R., and Franks, D. (1989). Healing potential of the anulus fibrosus. Spine *14*, 398–401. https://doi.org/10.1097/00007632-198904000-00009.
40. Torre, O.M., Mroz, V., Benitez, A.R.M., Huang, A.H., and Iatridis, J.C. (2019). Neonatal annulus fibrosus regeneration occurs via recruitment and proliferation of Scleraxis-lineage cells. NPJ Regen Med. *4*, 23. https://doi.org/10.1038/s41536-019-0085-4.
41. Soonpaa, M.H., Kim, K.K., Pajak, L., Franklin, M., and Field, L.J. (1996). Cardiomyocyte DNA synthesis and binucleation during murine development. Am. J. Physiol. *271*, H2183–H2189. https://doi.org/10.1152/ajpheart.1996.271.5.H2183.
42. Tang, S., Gantt, C., Salazar Puerta, A., Bodine, L., Khan, S., Higuita-Castro, N., and Purmessur, D. (2023). Nonviral overexpression of Scleraxis or Mohawk drives reprogramming of degenerate human annulus fibrosus cells from a diseased to a healthy phenotype. JOR Spine *6*, e1270. https://doi.org/10.1002/jsp2.1270.
43. Nakamichi, R., Ito, Y., Inui, M., Onizuka, N., Kayama, T., Kataoka, K., Suzuki, H., Mori, M., Inagawa, M., Ichinose, S., et al. (2016). Mohawk promotes the maintenance and regeneration of the outer annulus fibrosus of intervertebral discs. Nat. Commun. *7*, 12503. https://doi.org/10.1038/ncomms12503.
44. Panebianco, C.J., Dave, A., Charytonowicz, D., Sebra, R., and Iatridis, J.C. (2021). Single-cell RNA-sequencing atlas of bovine caudal intervertebral discs: Discovery of heterogeneous cell populations with distinct roles in homeostasis. FASEB J. *35*, e21919. https://doi.org/10.1096/fj.202101149R.
45. Yoshida, M., Nakamura, T., Sei, A., Kikuchi, T., Takagi, K., and Matsukawa, A. (2005). Intervertebral disc cells produce tumor necrosis factor alpha, interleukin-1beta, and monocyte chemoattractant protein-1 immediately after herniation: an experimental study using a new hernia model. Spine *30*, 55–61. https://doi.org/10.1097/01.brs.0000149194.17891.bf.
46. Iatridis, J.C.J.C., and ap Gwynn, I. (2004). Mechanisms for mechanical damage in the intervertebral disc annulus fibrosus. J. Biomech. *37*, 1165–1175. https://doi.org/10.1016/j.jbiomech.2003.12.026.
47. Travascio, F., Jackson, A.R., Brown, M.D., and Gu, W.Y. (2009). Relationship between solute transport properties and tissue morphology in human annulus fibrosus. J. Orthop. Res. *27*, 1625–1630. https://doi.org/10.1002/jor.20927.
48. Han, W.M., Anderson, S.E., Mohiuddin, M., Barros, D., Nakhai, S.A., Shin, E., Amaral, I.F., Pêgo, A.P., García, A.J., and Jang, Y.C. (2018). Synthetic matrix enhances transplanted satellite cell engraftment in dystrophic and aged skeletal muscle with comorbid trauma. Sci. Adv. *4*, eaar4008. https://doi.org/10.1126/sciadv.aar4008.
49. Barcellona, M.N., Speer, J.E., Fearing, B.V., Jing, L., Pathak, A., Gupta, M.C., Buchowski, J.M., Kelly, M., and Setton, L.A. (2020). Control of adhesive ligand density for modulation of nucleus pulposus cell phenotype. Biomaterials *250*, 120057. https://doi.org/10.1016/j.biomaterials.2020.120057.
50. Gilchrist, C.L., Darling, E.M., Chen, J., and Setton, L.A. (2011). Extracellular matrix ligand and stiffness modulate immature nucleus

pulposus cell-cell interactions. PLoS One *6*, e27170. https://doi.org/10.1371/journal.pone.0027170.

51. Ma, S.P., and Vunjak-Novakovic, G. (2016). Tissue-Engineering for the Study of Cardiac Biomechanics. J. Biomech. Eng. *138*, 021010. https://doi.org/10.1115/1.4032355.
52. Duclos, S.E., and Michalek, A.J. (2017). Residual strains in the intervertebral disc annulus fibrosus suggest complex tissue remodeling in response to in-vivo loading. J. Mech. Behav. Biomed. Mater. *68*, 232–238. https://doi.org/10.1016/j.jmbbm.2017.02.010.
53. Zhou, M., Lim, S., and O'Connell, G.D. (2021). A Robust Multiscale and Multiphasic Structure-Based Modeling Framework for the Intervertebral Disc. Front. Bioeng. Biotechnol. *9*, 685799. https://doi.org/10.3389/fbioe.2021.685799.
54. Iwatsuki, K., Cardinale, G.J., Spector, S., and Udenfriend, S. (1977). Reduction of blood pressure and vascular collagen in hypertensive rats by beta-aminopropionitrile. Proc. Natl. Acad. Sci. USA *74*, 360–362. https://doi.org/10.1073/pnas.74.1.360.
55. Panebianco, C.J., Rao, S., Hom, W.W., Meyers, J.H., Lim, T.Y., Laudier, D.M., Hecht, A.C., Weir, M.D., Weiser, J.R., and Iatridis, J.C. (2022). Genipin-crosslinked fibrin seeded with oxidized alginate microbeads as a novel composite biomaterial strategy for intervertebral disc cell therapy. Biomaterials *287*, 121641. https://doi.org/10.1016/j.biomaterials.2022.121641.
56. Howell, K.L., Kaji, D.A., Li, T.M., Montero, A., Yeoh, K., Nasser, P., and Huang, A.H. (2021). Macrophage depletion impairs neonatal tendon regeneration. Faseb. J. *35*, e21618. https://doi.org/10.1096/fj.202100049R.
57. Arvind, V., Howell, K., and Huang, A.H. (2021). Reprogramming adult tendon healing using regenerative neonatal regulatory T cells. Preprint at bioRxiv. https://doi.org/10.1101/2021.05.12.443424.
58. Aurora, A.B., Porrello, E.R., Tan, W., Mahmoud, A.I., Hill, J.A., Bassel-Duby, R., Sadek, H.A., and Olson, E.N. (2014). Macrophages are required for neonatal heart regeneration. J. Clin. Invest. *124*, 1382–1392. https://doi.org/10.1172/JCI72181.
59. Godwin, J.W., Debuque, R., Salimova, E., and Rosenthal, N.A. (2017). Heart regeneration in the salamander relies on macrophage-mediated control of fibroblast activation and the extracellular landscape. NPJ Regen. Med. *2*, 22. https://doi.org/10.1038/s41536-017-0027-y.
60. Rohanifar, M., Clayton, S.W., Easson, G.W.D., Patil, D.S., Lee, F., Jing, L., Barcellona, M.N., Speer, J.E., Stivers, J.J., Tang, S.Y., and Setton, L.A. (2022). Single Cell RNA-Sequence Analyses Reveal Uniquely Expressed Genes and Heterogeneous Immune Cell Involvement in the Rat Model of Intervertebral Disc Degeneration. Appl. Sci. *12*, 8244. https://doi.org/10.3390/app12168244.
61. Ribeiro-Machado, C., Santos, S.G., Amaral, I.A., Caldeira, J., Pereira, P., Barbosa, M.A., and Cunha, C. (2023). Macrophage-based therapy for intervertebral disc herniation: preclinical proof-of-concept. NPJ Regen. Med. *8*, 34. https://doi.org/10.1038/s41536-023-00309-z.
62. Hoy, R.C., D'Erminio, D.N., Krishnamoorthy, D., Natelson, D.M., Laudier, D.M., Illien-Jünger, S., and Iatridis, J.C. (2020). Advanced glycation end products cause RAGE-dependent annulus fibrosus collagen disruption and loss identified using in situ second harmonic generation imaging in mice intervertebral disk in vivo and in organ culture models. JOR Spine *3*, e1126. https://doi.org/10.1002/jsp2.1126.

STAR★METHODS

KEY RESOURCES TABLE

REAGENT or RESOURCE	SOURCE	IDENTIFIER
Antibodies		
Anti – Ki67	Abcam	Cat# Ab16667; RRID: AB_302459
Anti – CD45	Thermo Fisher	Cat# Pa5-96061; RRID: AB_2807863
Donkey Anti-Rabbit Cy5	Jackson Immuno Research	Cat# 711-175-152; RRID: AB_2340607
DAB Secondary Kit	Vector	Cat # MP-7801-15
Chemicals, peptides, and recombinant proteins		
BAPN	Sigma	A3134-SG
PBS	Thermo Fisher	BP399-20
PFA	Thermo Fisher	J19943-K2
EDTA	Fisher	5316–212
Sucrose	Thermo Fisher	A15583.0C
OCT	Thermo Fisher	4585
Mounting Medium	Electron Microscopy Sciences	16900
DAPI-containing Mounting Medium	Invitrogen	P36931
Picrosirius Red	Thermo Fisher	00059437
Alcian blue	Poly Scientific	S111A
Horse Serum	Vector	S-2012
RNAse Away	MBP	7002
Trizol	Invitrogen	15596018
Chloroform	Thermo Fisher	BP1145
Ethanol	Thermo Fisher	BP2818-500
Critical commercial assays		
ClickIt Edu Kit	Thermo Fisher	C10337
RNeasy Micro Kit	Qiagen	74004
Deposited data		
Bulk sequencing and analysis of mouse annulus fibrosus tissue	This paper	GEO: GSE275620
Experimental models: Organisms/strains		
C57bl/6J WT	The Jackson Laboratory	000664
C57bl/6j ScxGFP	Bred In house	Originated from Dr. Ronen Schweitzer
Software and algorithms		
ImageJ	National Inst. Of Health	https://imagej.nih.gov/nih-image/index.html
GraphPad Prism	Graphpad	https://www.graphpad.com/
Other		
26 G needle	BD	305111
27 G needle	Exel Int	26426
30 G needle	BD	305128
31 G needle	BD	328446
36 G needle	WPI	NF36BV
8-0 Prolene Sutures	Ethicon	873OH
Needle Stopper for 30 G	McMaster Car	20H304
Needle Stopper for 27/26 G	McMaster Car	21H304

(*Continued on next page*)

Continued

REAGENT or RESOURCE	SOURCE	IDENTIFIER
AFM Tips	Novascan	PT.PS
Phasemaker Tubes	Invitrogen	A33248
Blue India Ink	Thermo Fisher	3120124
Histological Slides	ASI	SM2575

EXPERIMENTAL MODEL AND STUDY PARTICIPANT DETAILS

Mice

Only mouse participants were used and no new human participants were recruited for this study. C57Bl6 mice were bred and maintained in house at Icahn School of Medicine within the Center for Comparative Medicine and Surgery (CCMS) with IACUC approval (Mount Sinai IACUC protocol #: IPROTO202100000042). C57Bl6 wildtype and *ScxGFP* transgenic reporter mice were used in this study including both males and females and ranging from age postnatal day 1 to skeletal maturity of 4–6 months old. Male and female *ScxGFP* reporter mice, originally generated by Dr. Ronen Schweitzer and bred in our colony, were distributed evenly by sex within each experimental group. Mice were housed in cages of up to 5 mice with 12-h light/dark cycles and had unlimited access to food and water.

METHOD DETAILS

BAPN Administration

β-aminopropionitrile (BAPN), a lysyl-oxidase inhibitor, was administered via drinking water (1 mg/mL) to pregnant females starting at embryonic day 5.5 and continued until mouse pups were postnatal day 5 (p5) or p14. The volume of drinking water consumed was monitored weekly to assess the average dose of BAPN ingested by the mice, which was similar to previous studies of BAPN in mice of ~5 mg of BAPN per mouse per day (~125 mg/kg per day).[15] Mice were euthanized at p5 or p14 for analysis. Additional p14 mice underwent AF puncture injury and were switched to regular water for the remaining 56 days after surgery until euthanasia.

Intervertebral disc herniation injury and mouse euthanasia

ScxGFP mice underwent coccygeal IVD puncture injuries.[11] Injuries on postnatal day 1 (p1), p5, p14, p28, and adult (4–6 months) mice were performed using a needle size ~80% IVD height and 50% IVD depth to induce herniation (Figure S1A). Needle sizes were adjusted for each age accounting for size differences at the time of injury (Figure S1B). Puncture needles were dipped in India Ink to visualize injured IVD levels. A total of 3–4 injuries were performed on alternating IVDs in on coccygeal levels cc4/5 and below with adjacent uninjured IVDs serving as internal controls. Coccygeal IVDs were located using *ScxGFP* expression through the skin using a stereo microscope with fluorescence capabilities (M60 microscope; Leica Microsystems). Neonatal p1 and p5 mice were anesthetized by placing in ice for puncture injuries. Neonatal p1 and p5 were punctured through the skin and did not require sutures. Mice aged p14 and p28 were anesthetized with isoflurane during puncture injury, with a small open microsurgical procedure (3–4 mm avoiding tendon). Sutures (8-0 prolene, Ethicon) closed incision sites and Buprenorphine administered (0.05 mg/kg). Control and injured IVDs were evaluated 3 days post-injury (d3) for injury severity assessments and d56 for regenerative assessments.

Tissue collection and processing

To assess regeneration, mice at either d3 (n = 3/experimental group) or d56 post-injury (n = 5/experimental group for histology, n = 7–9/experimental group for biomechanical analysis). Mice were euthanized by carbon dioxide inhalation and included UltraFocus Faxitron (Tucson, AZ, USA) imaging at d56 for IVD height. Another mice cohort with *in-vivo* injuries at p5 were evaluated at d84 to compare p5d56 and p5d84. For histology, tails were fixed in 4% paraformaldehyde (PFA), decalcified in ethylenediaminetetraacetic acid (EDTA), embedded in optimal cutting temperature (OCT) as vertebra–IVD–vertebra segments, and cryo-sectioned. Tails for biomechanical testing were stored in −80°C intact. Surgeries for each experimental group were performed in parallel (p1, p5, p14, p28, adult, and p14-BAPN) (Figure S1D). The p14d56 mice were compared with both p28d56 and 14BAPNd56 mice.

To characterize AF growth, C57BL6 wildtype mice were euthanized at postnatal day 1 (p1), p5, p14, p28, 2 months (p56), and 4–6 months (p112-p168) (n = 6–9/age) by decapitation or carbon dioxide inhalation. In parallel, additional mice underwent BAPN treatment until p5 or p14 (n = 6–9/experimental group) before euthanasia and were compared to their age matched untreated mice (Figure S1D). All groups were analyzed together; p5 and p14 mice were used in both the AF growth comparisons as well as in the BAPN studies against p5BAPN and p14BAPN. Tails used for AFM were stored in −80°C. Tails for immunohistochemistry and multiphoton imaging were unfixed and embedded immediately in OCT in multi-disc segments (p1, p5, p14, p5BAPN, p14BAPN) or as endplate-disc-endplate segments (p28, p56, and p112) to allow for sectioning without decalcification. Samples were cryo-sectioned into 20 μm sections and stored at 80°C. Additional p1-p8, p14, p28, p56, and adult (4–6 months) mice (n = 3/age) were used for cell proliferation assessment using EdU. 0.05 mg EdU was injected subcutaneously 2-h prior to sacrifice. Tails were fixed in 4% PFA, decalcified in EDTA, embedded in OCT as vertebra–IVD–vertebra segments, and cryo-sectioned.

Immunohistochemistry (IHC) and histology

To assess regeneration and evaluate gross morphology, samples were stained with picrosirius red (PR) for collagen and Alcian blue (AB) for glycosaminoglycans and imaged under brightfield light for % repair tissue within injury sites, IVD diameter, the number of AF lamellar layers and were imaged under polarized light to assign a collagen disorganization grade (Figure S2) for tissue near the injury sites. For fluorescence imaging, additional slides were stained with DAPI to visualize cell nuclei and *ScxGFP* expression for AF phenotype. Immunostaining was performed on additional slides using a rabbit anti-mouse CD45 primary (1:2400, Fisher Scientific, Cat# PA5-96061) and a DAB horse anti-rabbit secondary kit (Vector, MP-7801) with TolBlue counterstain to grade leukocytes staining. Cell proliferation was assessed within the anterior AF using EdU and immunohistochemistry against proliferation marker Ki67. EdU detection was performed using the Click IT EdU kit (Life Technologies), according to manufacturer instructions. For Ki67, primary anti-Ki67 (Abcam cat# Ab16667) (1:75) and a Cy5 secondary Ab (Jackson ImmunoResearch cat#711-175-152) (1:400) was used and slides were mounted using a DAPI-containing mounting medium (Prolong Gold Antifade with DAPI, ThermoFisher. Images were analyzed within ImageJ2 (version 2.3.0/1.53q) to count the total number of AF cells (DAPI) and the number of proliferating cells (Edu or Ki67) and presented as % AF cell proliferation. All images were taken at 10×, 20×, or 40× using an Axio Imager.Z1 microscope with an Apotome used for optical sectioning of fluorescent images (Zeiss, Thornwood, NY, USA). ImageJ2 was used to draw ROIs and for all cell counting.

Multiphoton imaging

Multiphoton imaging was performed on an Olympus FV1000 MPE laser-scanning microscope on mice from each age (n = 6–9/experimental group). Second harmonic generation (SHG) signal of fibrillar collagen and Two Photon Excitation Fluorescence (TPEF) signal of trivalent hydroxylysyl and trivalent lysyl pyridinoline crosslinks were imaged using an excitation at 910nm and 720nm for SHG and TPEF, respectively, and recorded by a photomultiplier tube at 440 ± 20nm.[17,62] Crosslinking density was found by normalizing TPEF crosslinking signal by SHG collagen signal as done previously.[17]

Atomic force microscopy (AFM)

On testing day, tails (n = 6–9/experimental group) were dissected and skin, tendon, and fascia removed. Remaining vertebra–IVD–vertebra samples were whole-mounted onto culture dishes with clear nail polish and covered with PBS to prevent dehydration. Using a biological AFM (MFP3D-BIO, Asylum Research), equipped with diving board shaped silicon probes (nominal spring constant, k = 7–9 N/m, calibrated individually) (Novascan) that had polystyrene spherical tips (diameter, d = 4.5 μm), the dorsal outer AF tissue stiffness was measured. Raw force-indentation measurements were acquired by indenting AF tissue at a rate of 12.5 μm/s until 100 nm of probe deflection was achieved, which equated to approximately 900 nN of force. To account for variability within each AF tissue, multiple indentations per sample were conducted, in an 8 × 2 arrays covering a 20 × 20 μm region of the AF. Raw force-depth curves from each indentation were fit using the Hertz model to calculate elastic modulus; data that did not fit well by the model were excluded based on the force-depth curves. Model calculations were dependent on each probe's calibrated spring constant (performed via the thermal noise method prior to each experiment) and assumed Poisson's ratio = 0.45. AFM control data analyses used Igor Pro (Wavemetrics Inc.).

Faxitron and disc height index (DHI)

Faxitron images were analyzed with ImageJ2 to calculate IVD height and vertebral length. (n = 7–9/experimental group). Three measurements were averaged for the height of each adjacent vertebrae and for the height of each disc. To calculate the DHI, the average disc height was normalized by the average of the two adjacent vertebral lengths. The DHI for each injured IVD was compared to the average DHI of the adjacent two uninjured control IVDs.

Biomechanical testing

For all biomechanical testing, mouse tails were removed immediately after euthanasia and stored in −80°C until testing day. On day of testing, two motion segments were removed from each tail, one injured, and one uninjured control. Levels cc4/5 and cc6/7 were used for testing with the level of the injured IVD varying between mice. Motion segments were cleaned of skin, tendon, and fascia before being potted in custom metal pots with superglue (with care taken to align vertebrae and IVD with the pots), followed by a 20-min rest period to rehydrate samples in PBS. Cyclical axial compression/tension and torsional testing was then performed on an ELF3200 axial and AR2000ex torsional rheometer respectively (TA instruments, New Castle, DE, USA). Motion segments were first subjected to 20 cycles of axial tension/compression to peak loads of ±0.5 N in displacement-control at 0.5 mm/s while submerged in PBS. After another 30-min resting period, motion segments were then transferred to the rheometer and underwent an equilibration of 5 min at 0.1 MPa axial stress to place the AF in circumferential tension before 20 cycles of torsion from ±20° at 0.5 Hz. Axial testing was analyzed for compressive stiffness, tensile stiffness, range of motion, and neutral zone length. Torsional testing was analyzed for torsional stiffness, torque range, and neutral zone length. Analyses were performed using MATLAB (MathWorks, Natick, MA, USA) code and plotted using GraphPad Prism (Version 9.4.1).

RNA extraction and bulk RNA-sequencing

Uninjured mice ages p5, p14, p21, and p28 (4 samples per age) were used for bulk RNA-seq. Each sample consisted of AF tissue from 2 to 3 tails from equivalently aged mice, with 8–10 discs/tail pooled. Care was taken to isolate AF tissue and discard NP and surrounding CEP. Each

sample was flash-frozen in liquid nitrogen followed by homogenization using a mikro-dismembrator (Sartorius; Göttingen, Germany). RNA extracted from homogenized AF tissue through the TRIzol/chloroform followed by RNeasy column kit (Qiagen). RNA quality and concentration analyzed using Nanodrop 2000 (ThermoFisher Scientific). All 16 samples sent to Azenta Life Sciences (South Plainfield, NJ) for DNase treatment, library preparation by rRNA depletion, sequencing (30 million reads per sample, Illumina NovaSeq6000), alignment, and principal component analysis and differential gene expression analyses. Gene set enrichment analysis (GSEA) was performed by submitting upregulated and downregulated DEGs (p value < 0.05, LFC>1 or LFC<−1) into Enrichr and analyzing GO ontologies (Biological Process 2021).

QUANTIFICATION AND STATISTICAL ANALYSIS

All statistical analyses used GraphPad Prism with significance for $p < 0.05$. Histological regeneration assessments (age window and BAPN) used $n = 5$ mice, functional measurements (DHI and biomechanical testing; age window and BAPN) used n = 6–9 mice. Growth characterization and BAPN effects on early growth used n = 6–9 mice. Shapiro-Wilk tested normality. Paired and unpaired Student's t-tests determined differences in DHI, % Repair tissue, Collagen Disorganization, Total # Cells, and % *ScxGFP*. For biomechanical testing, two-way ANOVA was used to first test the effect of interaction of age and surgery (control and injury) for regenerative window studies or for the interaction of treatment (p14 and p14BAPN) and surgery for the BAPN studies, followed by Student's t tests between control and injured IVDs for p14, p28, adult or p14BAPN. One way ANOVA with Tukey's Post-Hoc comparisons determined differences in collagen content, crosslinking, crosslinking density, AF modulus, and % cell proliferation with age. Student's t-tests determined differences in collagen content, crosslinking, crosslinking density, AF modulus, and % cell proliferation from BAPN treatment in p5 and p14 mice.